Geological Magazine

www.cambridge.org/geo

The Early Cretaceous tectonic evolution of the Neo-Tethys: constraints from zircon U–Pb geochronology and geochemistry of the Liuqiong adakite, Gongga, Tibet

Yao Zhong[1], Wen-Guang Yang[1], Li-Dong Zhu[1], Long Xie[1], Yuan-Jun Mai[1], Nan Li[1], Yu Zhou[1], Hong-Liang Zhang[2], Xia Tong[1] and Wei-Na Feng[3]

[1]Institute of Sedimentary Geology, Chengdu University of Technology, Chengdu 610059, China; [2]College of Earth Science, Chengdu University of Technology, Chengdu 610059, China and [3]The 106 Geological Brigade, Sichuan Bureau of Geology and Mineral Resources, Chengdu 611130, China

Original Article

Cite this article: Zhong Y, Yang W-G, Zhu L-D, Xie L, Mai Y-J, Li N, Zhou Y, Zhang H-L, Tong X, and Feng W-N (2022) The Early Cretaceous tectonic evolution of the Neo-Tethys: constraints from zircon U–Pb geochronology and geochemistry of the Liuqiong adakite, Gongga, Tibet. *Geological Magazine* **159**: 1647–1662. https://doi.org/10.1017/S0016756822000401

Received: 9 November 2021
Revised: 4 April 2022
Accepted: 22 April 2022
First published online: 13 June 2022

Keywords:
Gangdese; Neo-Tethys Ocean; Early Cretaceous; adakite; flat-slab subduction

Author for correspondence:
Wen-Guang Yang,
Email: yangwg1018@gmail.com

Abstract

The subduction model of the Neo-Tethys during the Early Cretaceous has always been a controversial topic, and the scarcity of Early Cretaceous magmatic rocks in the southern part of the Gangdese batholith is the main cause of this debate. To address this issue, this article presents new zircon U–Pb chronology, zircon Hf isotope, whole-rock geochemistry and Sr–Nd isotope data for the Early Cretaceous quartz diorite dykes with adakite affinity in Liuqiong, Gongga. Zircon U–Pb dating of three samples yielded ages of *c.* 141–137 Ma, indicating that the Liuqiong quartz diorite was emplaced in the Early Cretaceous. The whole-rock geochemical analysis shows that the Liuqiong quartz diorite is enriched in large-ion lithophile elements (LILEs) and light rare-earth elements (LREEs) and is depleted in high-field-strength elements (HFSEs), which are related to slab subduction. Additionally, the Liuqiong quartz diorite has high SiO_2, Al_2O_3 and Sr contents, high Sr/Y ratios and low heavy rare-earth element (HREE) and Y contents, which are compatible with typical adakite signatures. The initial $^{87}Sr/^{86}Sr$ values of the Liuqiong adakite range from 0.705617 to 0.705853, and the whole-rock $\epsilon_{Nd}(t)$ values vary between +5.78 and +6.24. The zircon $\epsilon_{Hf}(t)$ values vary from +11.5 to +16.4. Our results show that the Liuqiong adakite magma was derived from partial melting of the Neo-Tethyan oceanic plate (mid-ocean ridge basalt (MORB) + sediment + fluid), with some degree of subsequent peridotite interaction within the overlying mantle wedge. Combining regional data, we favour the interpretation that the Neo-Tethyan oceanic crust was subducted at a low angle beneath the Gangdese during the Early Cretaceous.

1. Introduction

The Qinghai–Tibet Plateau is a complex of multiple aggregated (micro) terranes with a long-term geological evolution (Yin & Harrison, 2000). The presence of several large ophiolite belts in the region is strong evidence of the existence of ancient oceans and the location of palaeoplate boundaries. Located in the southern margin of the Gangdese magmatic arc, the Yarlung–Zangbo Suture Zone (YZSZ) is generally regarded as a remnant of the Neo-Tethyan oceanic lithosphere that was subducted northward beneath the Lhasa terrane, with several ophiolitic remnants (fragments) distributed in a zonal pattern along the suture zone (Allègre *et al.* 1984; McDermid *et al.* 2002; Bédard *et al.* 2009; Zhou *et al.* 2015).

Subduction zones are dominant physical and chemical systems (Stern, 2002) that are vital for reconstructing the evolution of Earth. The subduction process of the Neo-Tethys Ocean has always been a controversial topic in geological research. To date, with continuous research data acquisition, different Early Cretaceous geodynamic models have been proposed: flat-slab (low-angle) subduction (Coulon *et al.* 1986; Ding & Lai, 2003; Kapp *et al.* 2005, 2007; Zhang *et al.* 2012; Wang *et al.* 2017), high-angle subduction (Zhu *et al.* 2009), intra-oceanic subduction (Aitchison *et al.* 2000; McDermid *et al.* 2002; Xu *et al.* 2009) and stable oblique subduction (Ji *et al.* 2009). Additionally, the beginning of the subduction of the palaeoplate has been proposed to be from the Late Triassic to the Early Cretaceous (Ji *et al.* 2009; Zhu *et al.* 2011; Kang *et al.* 2014; Huang *et al.* 2015; Zhong *et al.* 2016; XH Wang *et al.* 2021). Therefore, the exact timing of the Neo-Tethys subduction and evolution model during the Early Cretaceous is still inconclusive. In contrast to the central and northern regions of the Lhasa terrane, numerous studies have shown that there are only a few reports of Early Cretaceous magmatic rocks in the southern margin of the Lhasa terrane (Ji *et al.* 2009; Zhu *et al.* 2011), which might be one of the shortcomings in elucidating the evolution of the Neo-Tethys during the Early Cretaceous (Wang *et al.* 2017).

Defined by Defant and Drummond (1990), adakite refers to high-silicon, -Sr/Y and -La/Yb volcanic and intrusive rocks that are considered to be formed by the melting of young, hot, subducted slabs. However, recent studies have shown that adakitic rocks can be formed in different tectonic environments and by diverse mechanisms (Stern & Kilian, 1996; Zhang *et al.* 2002; Condie 2005; Wang *et al.* 2005; Guo *et al.* 2007; Shahbazi *et al.* 2021). Therefore, adakites have important research value for subduction zones, crustal thickening mechanisms and lower crustal evolution (Zhang *et al.* 2002).

Distributed in the Lhasa terrane, a large number of adakitic rocks (adakite) that erupted (or emplaced) in the Late Cretaceous and Cenozoic have been reported (Guan *et al.* 2010; Ma *et al.* 2013; Zheng *et al.* 2014; Chen *et al.* 2015; Lu *et al.* 2020; Wang *et al.* 2020), which record the evolution of the Neo-Tethys Ocean subduction and the geological history after the collision of the India–Eurasian plate. Many Late Cretaceous adakite rocks in the southern margin of the Lhasa terrane have gradually clarified the evolution of the Neo-Tethys during the Late Cretaceous (Wen *et al.* 2008; Guan *et al.* 2010; ZM Zhang *et al.* 2010; KJ Zhang *et al.* 2012; Ma *et al.* 2013; Zhao *et al.* 2013; Zheng *et al.* 2014; Chen *et al.* 2015; Xu *et al.* 2015; Dai *et al.* 2018). In contrast, there are only a handful of reports on Early Cretaceous adakite (or adakitic) rocks (Yao *et al.* 2006; Kang *et al.* 2009; Zhu *et al.* 2009). Accordingly, to better constrain the evolution model of the Neo-Tethys during the Early Cretaceous, more data are needed.

Here, we report new zircon U–Pb geochronology, zircon Hf isotope analyses, whole-rock geochemistry and Sr–Nd isotope results for the Early Cretaceous adakitic quartz diorite rocks that occur in the Liuqiong and Gongga areas along the southern margin of the Gangdese magmatic arc. We discuss the petrogenesis, magma evolution and tectonic significance of the Early Cretaceous adakite, providing new data for elucidating the Neo-Tethys evolution during the Early Cretaceous.

2. Geological setting

The Qinghai–Tibet Plateau, which is also referred to as 'the combined plateau' (Dewey, 2005; Xu *et al.* 2006; Fig. 1a), is essentially composed of four blocks: the Songpan–Ganzi, Qiangtang, Lhasa and Himalayan terranes, from north to south (Yin & Harrison, 2000). The Lhasa terrane (Gangdese) is an E–W-extending structure-magmatic belt that is ~100–300 km wide and 2500 km long (Pan *et al.* 2006; Zhu *et al.* 2006). As the southern and northern boundaries of the Lhasa terrane, the YZSZ and the Bangong–Nujiang Suture Zone (BNSZ) are remnants of the oceanic crust after the closure of the Yarlung–Zangbo Ocean and Bangong–Nujiang Ocean, respectively (Fig. 1b). Due to the influence of the ancient oceans on both sides of the Lhasa terrane, Mesozoic magmatism is widespread in this region. The internal magmatic rocks become younger from south to north, reflecting the northward migration of magmatic activity, which might be the product of the northward subduction of the Neo-Tethys (Chu *et al.* 2006; Ji *et al.* 2009). However, some scholars believe that the Mesozoic magmatism in the Lhasa terrane is mainly related to the southward subduction of the Bangong–Nujiang Ocean, but the effect of this subduction system may have been minimal in the Early Cretaceous (Zhu *et al.* 2011). Considering the large distance between the southern margin of the Gangdese and the BNSZ before crustal shortening and deformation (caused by the subduction of the Bangong–Nujiang Ocean in the north and the Neo-Tethys Ocean in the south and the collision between Qiangtang and the Lhasa and Himalayan terranes), the magmatic activity near the southern margin of the Gangdese is more likely to be the product of the northward subduction of the Neo-Tethys (Zhu *et al.* 2011).

Focusing on Cretaceous magmatism, we note that Early Cretaceous magmatism is widely distributed in the central and northern parts of the Gangdese but is extremely rare in its southern area (Zhu *et al.* 2006; Ji *et al.* 2009). The magmatic rocks in the southern margin of the Gangdese erupted (or were emplaced) in the Late Cretaceous (Fig. 1b). Recently, the increase of Early Cretaceous magmatic rocks reported within the southern margin of the Gangdese has pushed the study of the subduction model of the Neo-Tethys during the Early Cretaceous to the forefront once again (Kang *et al.* 2009; Zhu *et al.* 2009; Wang *et al.* 2017).

3. Field occurrence and petrography

The study area is located in Liuqiong village, *c.* 5 km from the north bank of the Yarlung–Zangbo River. Late Cretaceous magmatic rocks and a small amount of Early Cretaceous volcanic rocks are exposed in the study area (Wang *et al.* 2017). Additionally, geological mapping surveys have indicated that large-scale Eocene intrusive rocks are exposed towards the northwest (Fig. 1c). The Upper Triassic Changguo Formation (T_3cg), Upper Triassic – Lower Jurassic Liuqiong Formation (T_3J_1l), Upper Jurassic – Lower Cretaceous Linbuzong Formation (J_3K_1l), Lower Cretaceous Takena Formation (K_1t) and Palaeocene Dianzhong Formation (E_1d) are the main component units (Fig. 1c). The Liuqiong Formation (T_3J_1l) features a complex rock assemblage, mainly including basalt, volcanic breccia, breccia crystalline tuff, limestone, breccia limestone and tuffaceous siltstone (Fig. 2). Whole-rock geochemical characteristics indicate that the volcanic rocks within the Liuqiong Formation have arc setting signatures (GM Li *et al.* 2020). The sedimentary environment and provenance characteristics of clastic rocks indicate that the Liuqiong Formation was deposited in a fore-arc basin on the southern margin of Gangdese (N Li, unpub. Master's thesis, Cheng Univ. of Technology, 2021). During the field geological survey, two porphyritic quartz diorite dykes were discovered (note: Samples D0085 and D0087 were collected from the same dyke of section A, while sample 20CG21 was collected from another dyke of section B (Figs 1c and 2)). It is clear that the porphyritic quartz diorite dykes are intrusive into the Liuqiong Formation (Figs 2 and 3); the intrusive contact between the dykes and the surrounding rocks of the Liuqiong Formation is shown in Figure 3.

The fresh surface of the Liuqiong quartz diorite dyke is light grey, and there is no obvious phenomenon of later weathering. The investigated rocks are characterized by a porphyritic texture, with phenocrysts mainly composed of grey–white plagioclase, flesh-red alkali feldspar, dark long prismatic hornblende and a small amount of granular quartz (Fig. 3c and f). The particle size of the phenocrysts is mostly *c.* 1 mm in diameter, and the diameter of certain phenocrysts may be in the 2–3 mm range (Fig. 4). Most phenocrysts of hornblende and feldspars are altered, forming pits and holes in both the edge and core/nucleus of the minerals. The groundmass matrix shows a fine-microcrystalline texture, mainly composed of microcrystalline plagioclase, amphibole and quartz crystals (Fig. 4). According to the strong alteration observed in the thin-section of sample 20CG21 (Fig. 4d–f), whole-rock Sr–Nd isotope analysis was conducted for the dyke from section A only.

https://doi.org/10.1017/S0016756822000401 Published online by Cambridge University Press

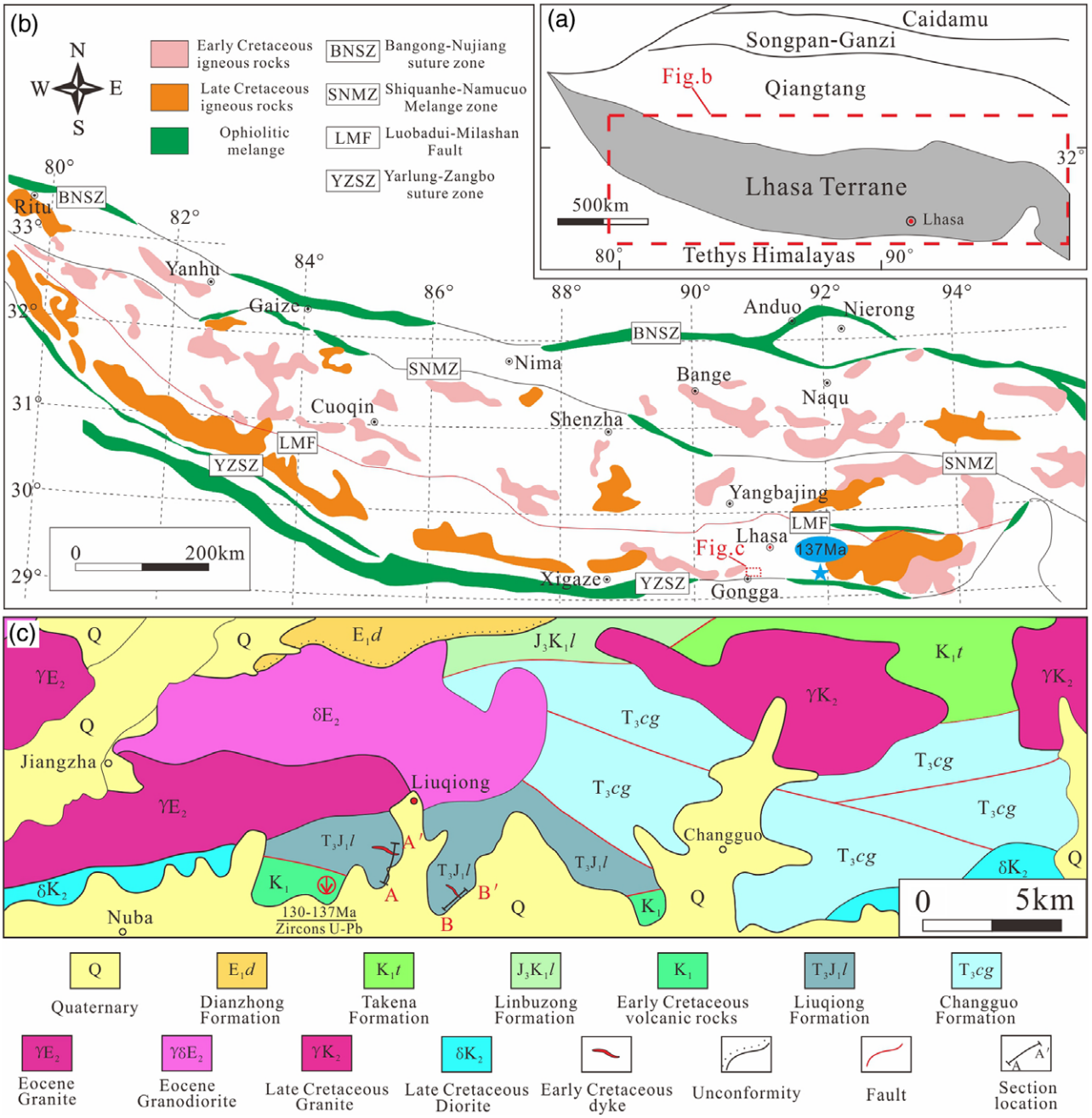

Fig. 1. (Colour online) (a) Tectonic outline of the Tibetan Plateau. (b) The distribution of Cretaceous magmatism (modified from Zhu *et al.* 2011; Mamen adakite-like rocks are cited from Zhu *et al.* 2009). (c) Geological sketch of the study area (modified from a regional geological map with a scale of 1:50 000; Early Cretaceous volcanic rocks are cited from Wang *et al.* 2017).

4. Analytical techniques

4.a. Whole-rock geochemical analyses

Major and trace element analyses were performed at Wuhan Sample Solution Analytical Technology Co., Ltd, in Wuhan, China. Whole-rock major element analysis was conducted on an X-ray fluorescence (XRF) instrument (Primus II, Rigaku, Japan), and trace element analysis was conducted on an Agilent 7700e ICP-MS (inductively coupled plasma – mass spectrometry) instrument. Whole-rock Sr–Nd isotopes were determined at Beijing GeoAnalysis Technology Co., Ltd. Isotopic composition analyses of Sr and Nd were undertaken using a Thermo Fisher Scientific Neptune Plus multi-collector MC-ICP-MS. $^{87}Sr/^{86}Sr$ ratios were corrected for instrumental mass fractionation using the exponential fractionation law and assuming $^{88}Sr/^{86}Sr = 8.375209$. $^{143}Nd/^{144}Nd$ ratios were corrected for instrumental mass fractionation using the exponential fractionation law and assuming $^{146}Nd/^{144}Nd = 0.7219$. For the analytical details, refer to Yang *et al.* (2005). The whole-rock major and trace element data and Sr–Nd isotope results are listed in Table S1 (in the Supplementary Material available online at https://doi.org/10.1017/S0016756822000401).

https://doi.org/10.1017/S0016756822000401 Published online by Cambridge University Press

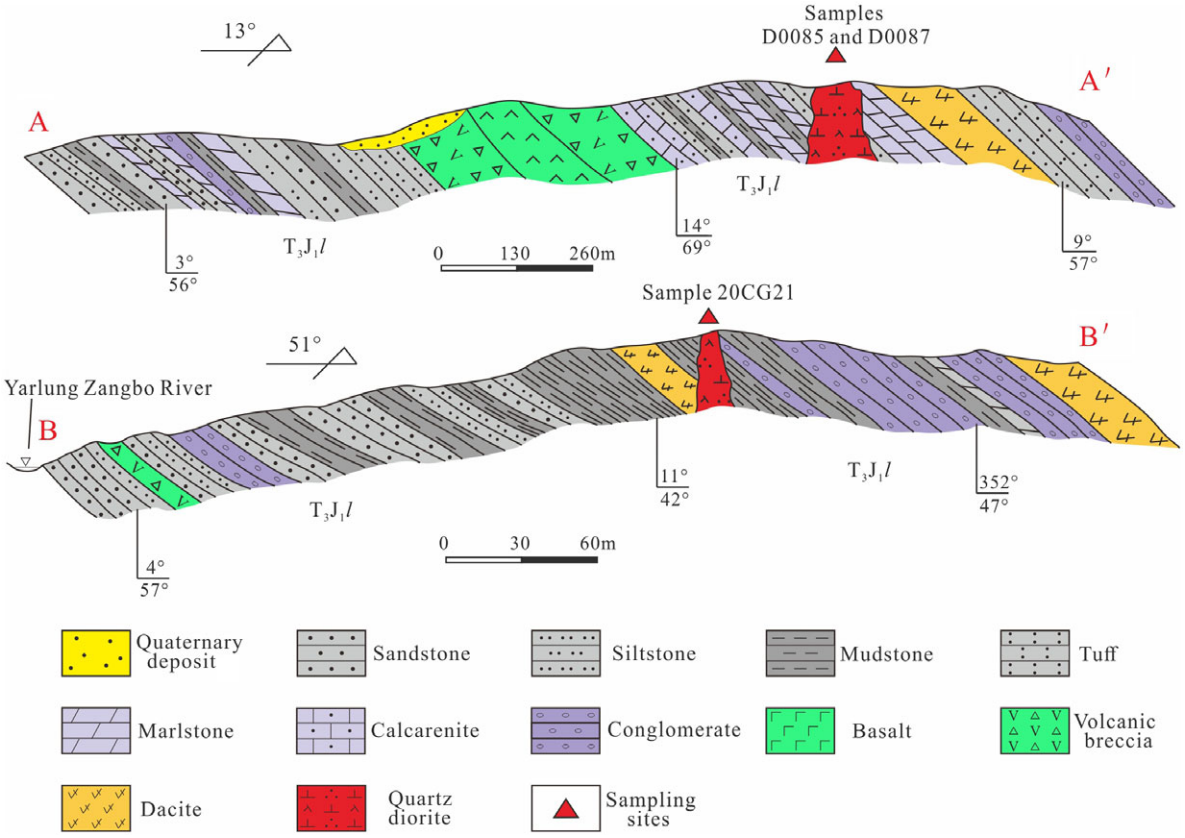

Fig. 2. (Colour online) Schematic cross-sections.

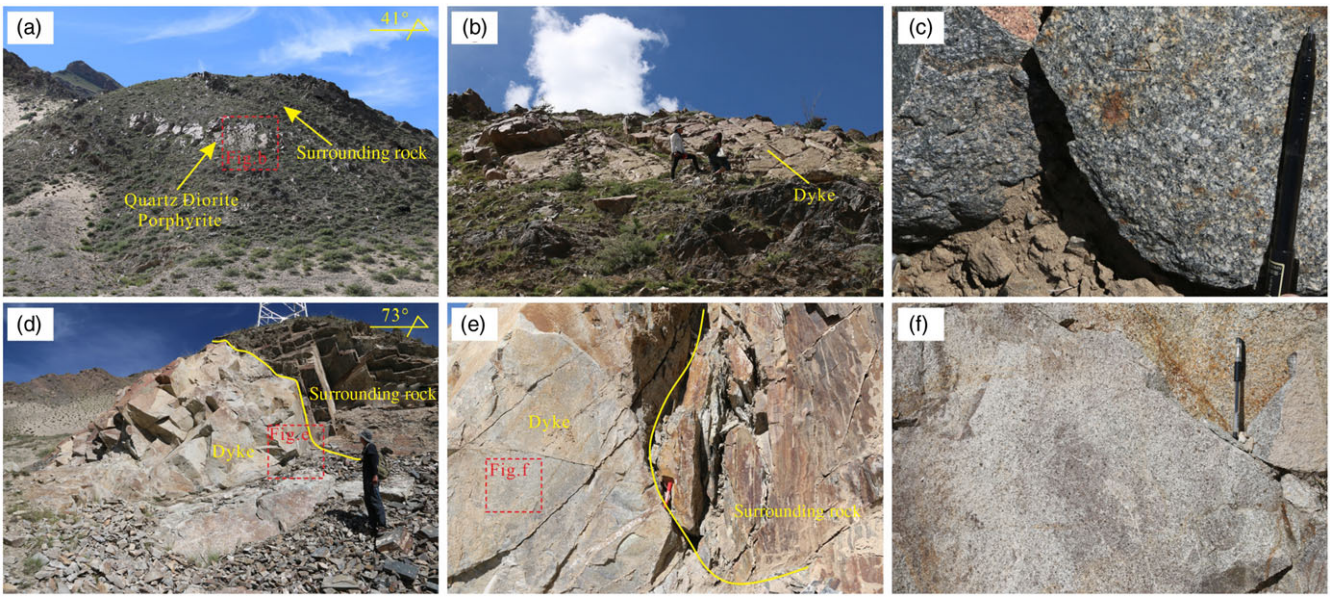

Fig. 3. (Colour online) Field photographs of the quartz diorite. (a, b, d, e) The contact relations of the quartz diorite and surrounding rocks. (c, f) Fresh surfaces of quartz diorite.

4.b. Zircon U–Pb dating

Zircon U–Pb dating was conducted using LA-ICP-MS at the Beijing GeoAnalysis Technology Co., Ltd. The Resolution SE model laser ablation system (Applied Spectra, USA) was equipped with an ATL (ATLEX 300) excimer laser. The laser ablation system was coupled to an Agilent 7900 ICP-MS (Agilent, USA). Details about the tuning parameters are provided in Thompson *et al.* (2018). The analyses were performed using a 30 μm diameter spot at 5 Hz and a fluence of 2 J cm^{-2}. Zircons 91500 (~1062 Ma) and GJ-1 (~602 Ma) were utilized as reference materials. NIST 610 and ^{91}Zr were selected to calibrate the trace element concentrations as external reference materials and internal standard elements,

https://doi.org/10.1017/S0016756822000401 Published online by Cambridge University Press

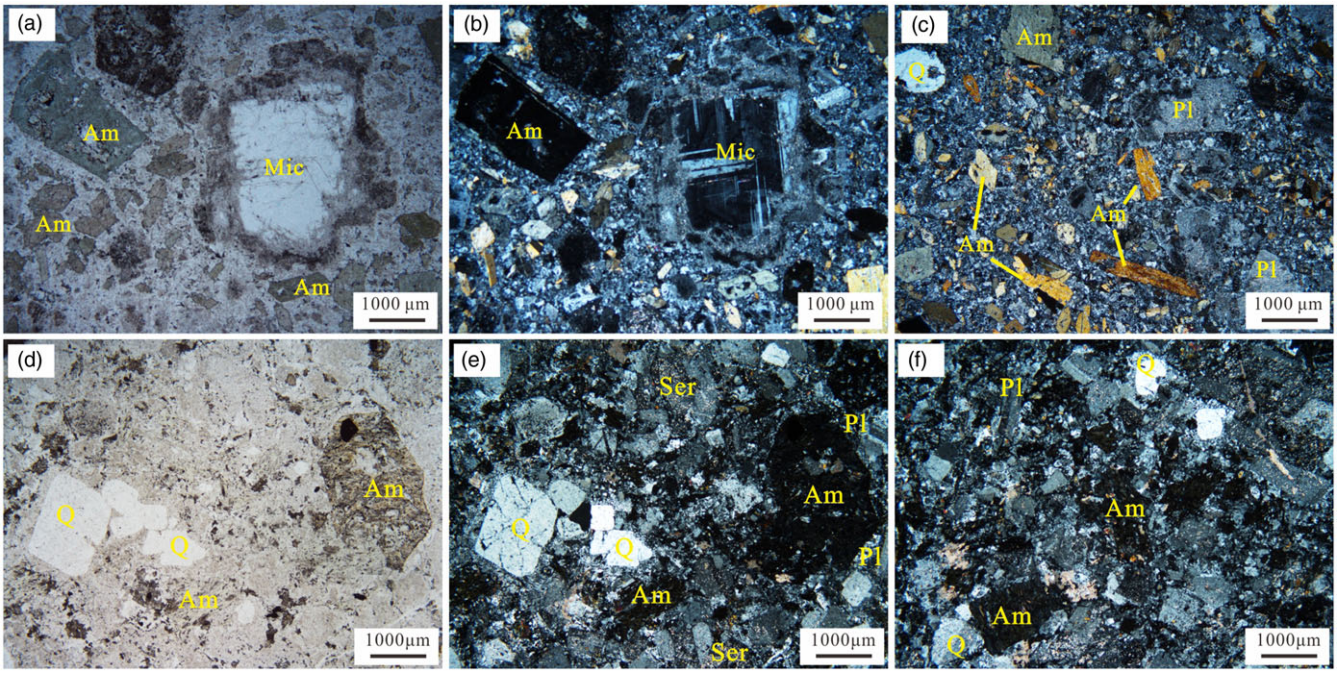

Fig. 4. (Colour online) Microphotographs. (a, b) Phenocrysts in diorite D0087. (c) The matrix in the porphyritic texture (D0087). (d, e) Altered amphibole phenocrysts in the diorite of 20CG21. (f) Matrix composed of fine-grained minerals (20CG21). Abbreviations: Am – amphibole; Mic– microcline; Q – quartz; Pl – plagioclase; Ser – sericite.

respectively. Common Pb was corrected following the method of Andersen (2002). Zircon U–Pb ages are given in Table S2 and Figure S1 in the Supplementary Material available online at https://doi.org/10.1017/S0016756822000401. Isoplot/Ex_ver 3 was used to calculate the U–Pb age and the weighted average age of the samples (Ludwig, 2003).

4.c. Zircon Lu–Hf isotope analyses

In situ zircon Lu–Hf isotope ratio analysis experiments were conducted using a Neptune Plus LA-MC-ICP-MS coupled with an ESI NWR LA system (193 nm) at Beijing GeoAnalysis Technology Co., Ltd. The laser beam diameter was 40 μm, the energy density was 5 J cm^{-2} and the frequency was 8 Hz. The measured $^{176}Hf/^{177}Hf$ ratios were normalized to $^{179}Hf/^{177}Hf = 0.7325$. The operational conditions, detailed analysis procedures and data correction methods are described in Wu *et al.* (2006). Zircon Hf isotope data are shown in Table S3, and reference materials are plotted in Figure S2, in the Supplementary Material available online at https://doi.org/10.1017/S0016756822000401.

5. Results

5.a. Geochemistry

Whole-rock geochemical data of Liuqiong quartz diorites are shown in Table S1 (in the Supplementary Material available online at https://doi.org/10.1017/S0016756822000401). The samples show varying degrees of alteration based on their petrographical characteristics and loss on ignition (LOI). One of the dykes does not show evidence of remarkable alteration (with a low LOI, samples D0087). The second dyke (samples 20CG21), however, has undergone stronger late alteration based on the high LOI values (ranging between 3.57 and 4.36 wt %). All of the samples have high SiO_2 (*c.* 60 wt %) and Al_2O_3 (16.37–16.85 wt %) contents. All samples are classified as diorite in the total alkali versus silica (TAS) plot (Fig. 5a), and in the classification plot of SiO_2 versus K_2O, they plot in the low-K tholeiite field (Fig. 5b). The diorite samples contain 2.77–4.55 wt % MgO, and the $Mg^{\#}$ ranges from 58 to 66, indicating no obvious fractionation.

The trace element compositions of the quartz diorite are characterized by the pronounced fractionation of light and heavy rare earth elements (LREEs and HREEs) (Fig. 6a). The total rare earth element contents (∑REE) of the samples are between 62 ppm and 79 ppm, with an average of 70 ppm. The LREE contents range from 54 ppm to 70 ppm, and the HREE contents are extremely low, with an average of 8 ppm. The LREE/HREE ratios are in the range 6.49 to 8.69, with an average $(La/Yb)_N$ ratio of 7.79, indicating prominent fractionation of LREEs over HREEs. There are no obvious Ce and Eu anomalies (Fig. 6a). In the primitive-mantle-normalized plot, the Liuqiong quartz diorite exhibits considerable enrichment in large ion lithophile elements (LILEs) and negative Nb–Ta anomalies, which may suggest an affinity with magmas generated in a subduction-related tectonic setting (Zhu *et al.* 2009).

Notably, the Liuqiong quartz diorites display low concentrations of HREEs, Y and Yb (Y = 11.1–13.02 ppm, Yb = 1.11–1.27 ppm). In contrast, the samples are enriched in LREEs and Sr (774–1099 ppm). These characteristics, in conjunction with high Sr/Y ratios (63–93), indicate that these samples could be classified as adakites, according to the definition of Defant & Drummond (1990) (Fig. 7). Overall, the REE patterns and the spider plot of trace elements of Liuqiong quartz diorite resemble those of the Mamen adakite-like rocks reported by Zhu *et al.* (2009) and the widespread Late Cretaceous adakite-like rocks in the Lhasa terrane (Figs. 6 and 7).

Whole-rock Sr–Nd isotope data for five samples from the Liuqiong quartz diorite are listed in Table S1 (in the Supplementary Material available online at https://doi.org/10.1017/S0016756822000401). The initial $^{87}Sr/^{86}Sr$ and $^{143}Nd/^{144}Nd$

https://doi.org/10.1017/S0016756822000401 Published online by Cambridge University Press

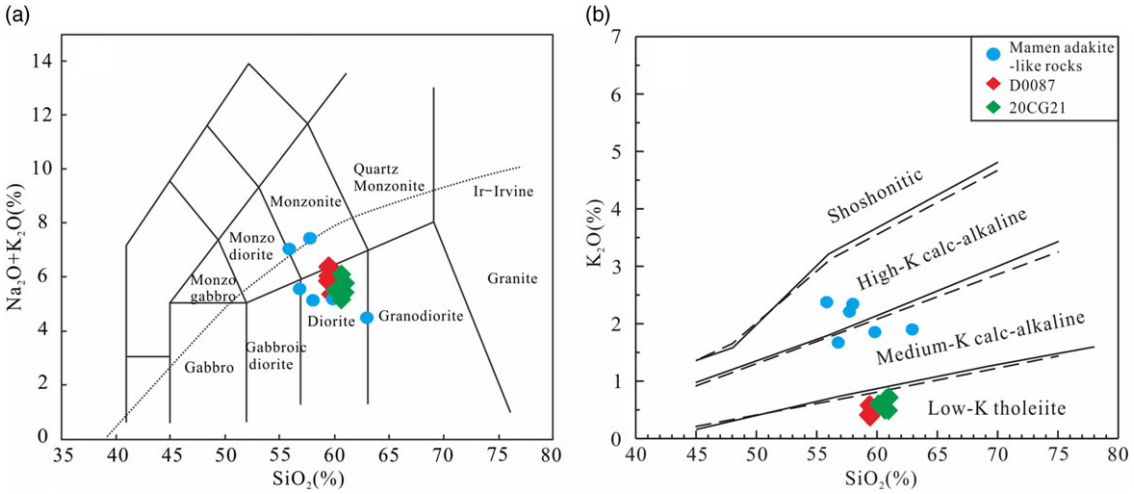

Fig. 5. (Colour online) The total alkali versus silica plot (Middlemost, 1994) (a) and SiO_2 versus K_2O classification plot (Rollinson, 1993) (b) of the Liuqiong quartz diorite. Data of Mamen adakite-like rocks are cited from Zhu *et al.* (2009).

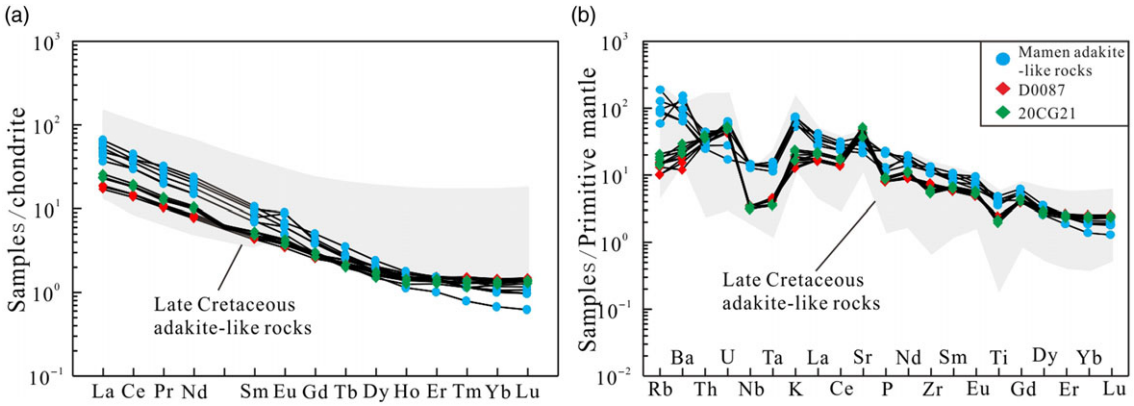

Fig. 6. (Colour online) Chondrite-normalized REE patterns (a) and primitive-mantle-normalized trace element spider plots (b) for the Liuqiong quartz diorite. The chondrite values and primitive-mantle values are cited from Sun & McDonough (1989). Data of the Late Cretaceous are cited from Guan *et al.* (2010), Zhang *et al.* (2010), Ma *et al.* (2013) and Xu *et al.* (2015).

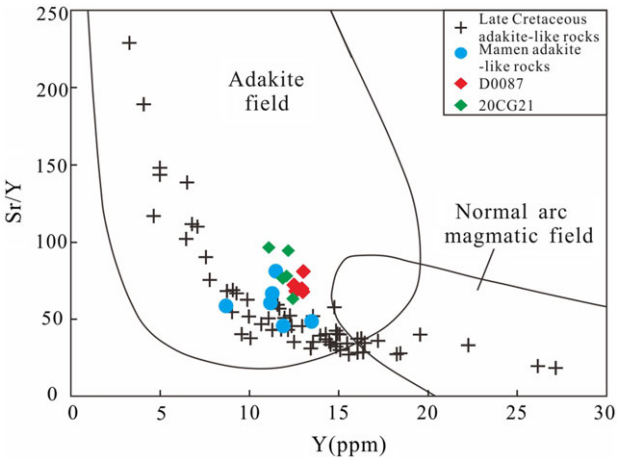

Fig. 7. (Colour online) Sr/Y–Y plot for the Liuqiong quartz diorite (after Defant & Drummond, 1990). Data are from the same source as in Fig. 6.

ratios and $\epsilon_{Nd}(t)$ values were calculated based on the zircon U–Pb ages (*c.* 141 Ma) obtained in our study (refer to Section 5.b). All five samples have relatively homogeneous Sr and Nd isotope compositions. As shown in Table S1, the initial $^{87}Sr/^{86}Sr$ ratios of rocks range from 0.705617 to 0.705853, and the samples have moderately positive $\epsilon_{Nd}(t)$ values (+5.78 to +6.24) (figure not shown; refer to Table S1).

5.b. Zircon U–Pb geochronology

To obtain the precise ages of the Liuqiong quartz diorite, three samples were collected (D0085-N3, D0087-N1 and 20CG21-N5). In the cathodoluminescence (CL) images of zircons obtained (Fig. 8), all samples have similar morphological characteristics, and most zircons are euhedral, prismatic crystals and transparent. The typical oscillatory zoning within the zircons shown in the CL images, with no resorption or inherited cores, indicates that they have a magmatic origin. The zircons vary from 110 to 180 μm in length and 40 to 100 μm in width; thus, the ratios of the two are *c.*

https://doi.org/10.1017/S0016756822000401 Published online by Cambridge University Press

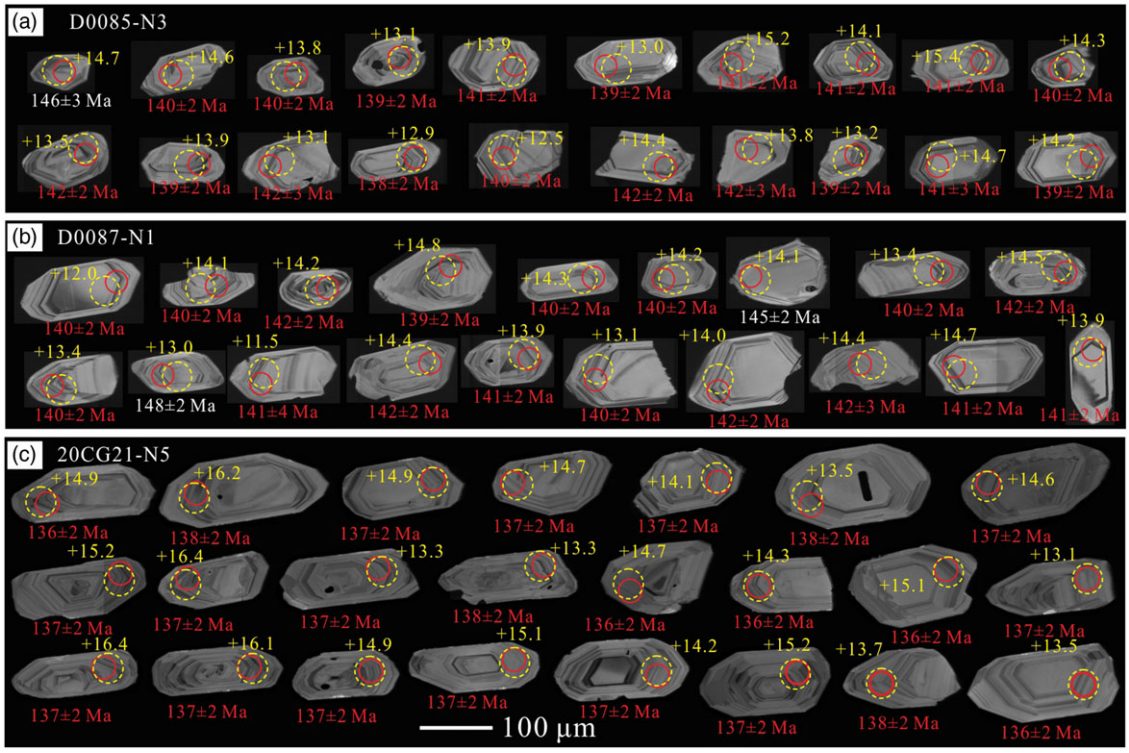

Fig. 8. (Colour online) CL images of zircon grains analysed in this study.

3:1 to 1:1. Twenty, 20 and 23 zircons were analysed for samples D0085-N3, D0087-N1 and 20CG21-N5, respectively. All the results obtained are listed in Table S2 (in the Supplementary Material available online at https://doi.org/10.1017/S0016756822000401). Twenty, 19 and 23 valid data points were obtained after removing the spots with low concordance (<90 %). The Th/U ratios of these zircons range from 0.32 to 0.83 (average of 0.46) (most of the results are greater than 0.4), also indicative of a magmatic origin for the investigated zircons (Belousova *et al.* 2002; Hoskin & Black, 2010). Therefore, the zircon ages can be regarded as representative of the time of emplacement of the Liuqiong quartz diorite.

Twenty analytical spots on zircons from sample D0085-N3 yielded concordant $^{206}Pb/^{238}U$ ages of 138.4 ± 2.1 to 145.5 ± 2.5 Ma, with a weighted mean age of 140.2 ± 0.5 Ma (n = 19, MSWD = 1.5) (Fig. 9a, b). Nineteen analytical spots on zircons from sample D0087-N1 yielded concordant $^{206}Pb/^{238}U$ ages between 138.9 ± 1.8 and 147.5 ± 2.0 Ma, with a weighted mean age of 140.7 ± 0.5 Ma (n = 17, MSWD = 0.95) (Fig. 9c, d). For sample 20CG21-N5, similar ages were obtained from 23 analytical spots, with a weighted mean age of 137.1 ± 0.9 Ma (n = 23, MSWD = 0.09) (Fig. 9e, f). The aforementioned results indicate that the Liuqiong quartz diorite was emplaced in the Early Cretaceous.

5.c. Hf isotopes

Hf isotope analysis was performed on (near) the zircon spots for U–Pb dating. (Fig. 8). The results are shown in Table S3 (in the Supplementary Material available online at https://doi.org/10.1017/S0016756822000401). The results show that all $^{176}Lu/^{177}Hf$ values of the investigated samples are below 0.002 and that the measured $^{176}Hf/^{177}Hf$ values could represent the Hf isotopic composition of the system during zircon formation (Amelin *et al.* 1999; Hou *et al.* 2007; Wu *et al.* 2007). The zircon $\epsilon_{Hf}(t)$ values vary from +12.5 to +15.4 for sample D0085-N3, +11.5 to +14.8 for sample D0087-N1, and +12.7 to +16.0 for sample 20CG21-N5 (Fig. 10). The single-stage Hf model ages (T_{DM1}) and two-stage Hf model ages (T_{DM2}) range between 166–283 Ma and 181–368 Ma for sample D0085-N3, between 190–323 Ma and 220–433 Ma for sample D0087-N1, and between 137–273 Ma and 137–353 Ma for sample 20CG21-N5.

6. Discussion

6.a. Alteration effects

According to the whole-rock, geochemical and microscopic characteristics, some of the investigated samples have undergone alteration (especially sample 20CG21). Therefore, it is necessary to estimate the mobility of the elements before discussing the petrogenesis and source properties of the elements. Some LILEs (Sr, Rb, etc.) often migrate during alteration, so it is not suitable to consider them in further analysis and discussion. In contrast, REEs and high-field-strength elements (HFSEs) are relatively stable (Th, Nb, Ta, Zr, Hf, Y, etc.) (Rollinson, 1993). Binary plots versus LOI are employed as proxies for alteration intensity (Wang *et al.* 2016), and the correlation coefficient R = 0.75 is the critical point for element mobility (Polat & Hofmann, 2003). In this work, the correlations between REEs (Th, Nd, Nb, Ta, La, Gd, Yb, Sm, etc.) that are commonly employed for the discussion of petrogenesis and source regions are generally weak (correlation coefficients are mostly below 0.75; figures not shown), which indicates that these elements can remain stable (or almost stable) during the process of alteration. Additionally, previous studies have already demonstrated that Zr, Hf, Fe, A1, Th, Nb, Sc and REEs are

https://doi.org/10.1017/S0016756822000401 Published online by Cambridge University Press

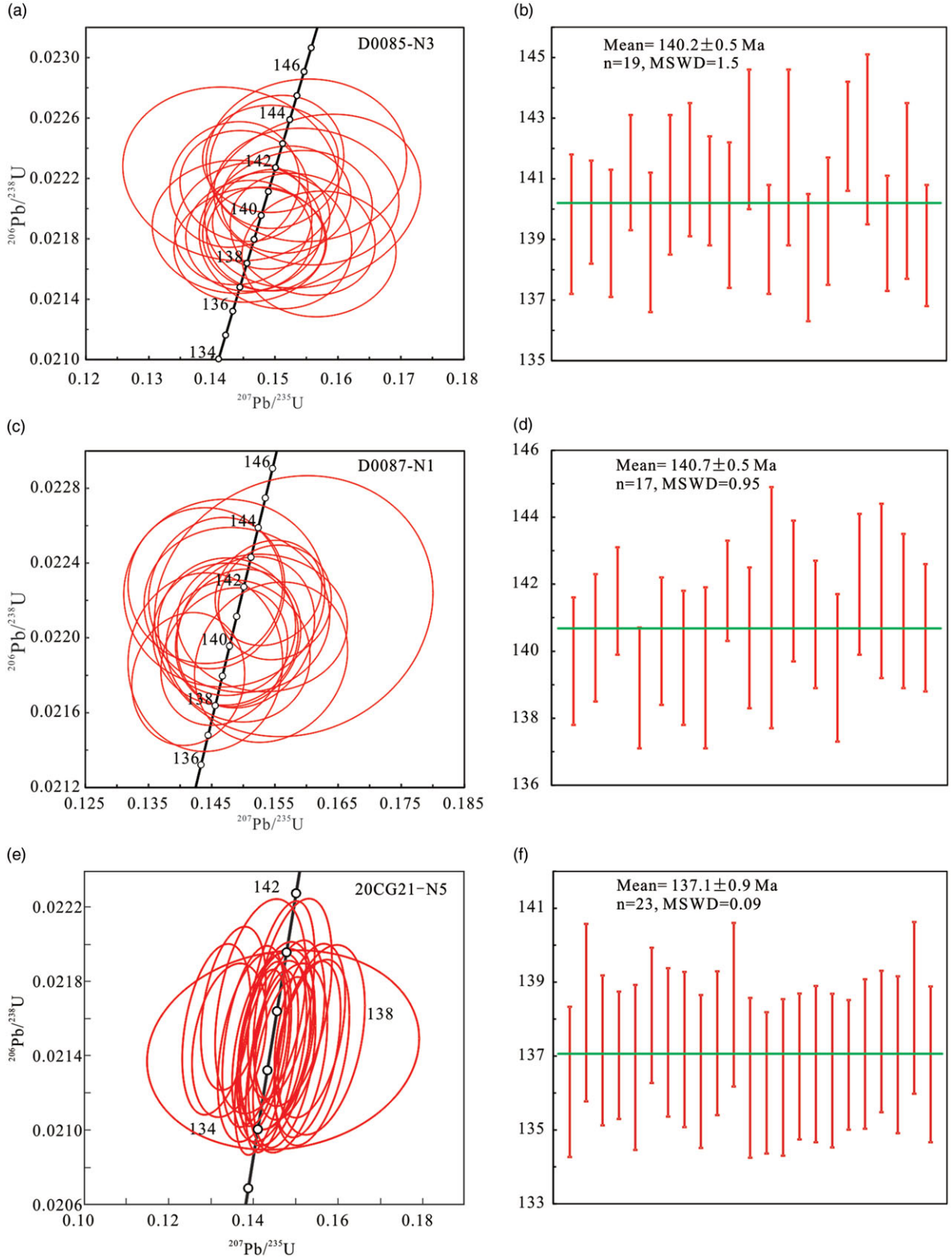

Fig. 9. (Colour online) U–Pb age concordia plots.

https://doi.org/10.1017/S0016756822000401 Published online by Cambridge University Press

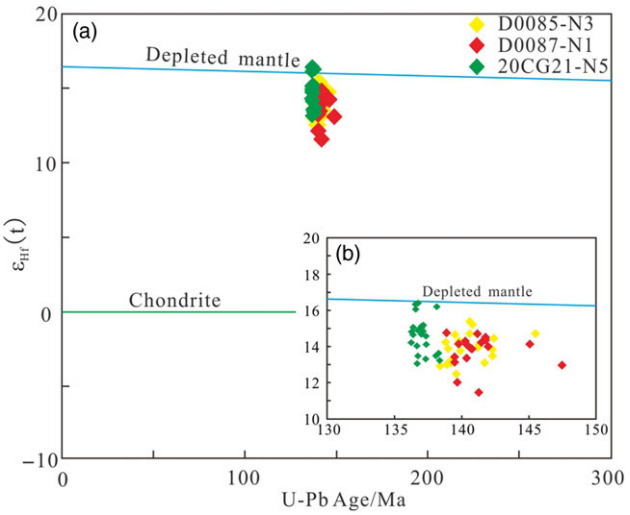

Fig. 10. (Colour online) $\epsilon_{Hf}(t)$ versus U–Pb age plot for zircons.

immobile during weathering (Middelburg *et al.* 1988). Consequently, these immobile elements are utilized for subsequent discussion.

6.b. Petrogenesis

According to its unique geochemical characteristics, adakite was defined as a volcanic or intrusive rock formed by partial melting of a young (<25 Ma) and hot oceanic crust when first reported (Defant & Drummond, 1990). Currently, it is proposed that adakite rocks form in different tectonic environments by diverse mechanisms. The main viewpoints about the petrogenesis of adakites include partial melting of the subducted continental crust (Lai & Qin, 2013), partial melting of the (thickened) lower crust (Atherton & Petford, 1993; Chung *et al.* 2003; Hou *et al.* 2004; Wang *et al.* 2005; Long *et al.* 2015; Shahbazi *et al.* 2021), mixing of felsic and basaltic magma (Guo *et al.* 2007; Streck *et al.* 2007), crystallization differentiation of basaltic magma (including low-pressure, fractional crystallization of plagioclase and amphibole, and high-pressure, fractional crystallization involving amphibole and garnet) (Castillo *et al.* 1999; Gao *et al.* 2009; Dai *et al.* 2018), and partial melting of subducting oceanic crust (Defant & Drummond, 1990; Wang *et al.* 2007).

Numerous studies have limited the collision time between the Indian continent and the Asian continent to the range of ~60–50 Ma through multidisciplinary studies (Najman *et al.* 2017 and references therein); that is, the southern margin of the Lhasa terrane did not undergo the evolutionary process of continental crust subduction. In this case, the Liuqiong adakite could not be attributed to partial melting of the subducted continental crust. The SiO_2 contents of the Liuqiong adakite are generally high (all *c.* 60 wt %), and there are no basic enclaves within the dykes. Adakitic rocks formed by the mixing of dacitic and basaltic magmas usually have high MgO contents (>4.5 wt %) and $Mg^{\#}$ values (>66; Wang *et al.* 2006). The results of our study reveal that only some samples have high MgO and $Mg^{\#}$ values (4.37 wt % and 64.8 on average, respectively), which are not attributed to adakites derived from a mixture of dacitic and basaltic magmas (Table S1, in the Supplementary Material available online at https://doi.org/10.1017/S0016756822000401). The above characteristic hampers the process of mixing between dacitic and basaltic magmas as the Liuqiong adakite source (Dong *et al.* 2020; B Wang *et al.* 2021).

In the Sm–La/Sm and La–$(La/Yb)_N$ plots (Fig. 11), the investigated samples plot close to each other, showing no trend of fractional crystallization or partial melting. However, considering the limitation of our research data, we take into account the coeval Mamen adakite (136.5 ± 1.7 Ma) (Zhu *et al.* 2009). As shown in Fig. 11, these Early Cretaceous adakites exhibit an obvious trend of partial melting. In combination with the homogeneous values of the whole-rock, Sr–Nd isotopes and zircon Hf isotope compositions (Fig. 10), we conclude that the Liuqiong adakite cannot be the fractional crystallization product of a more primitive magma (Long *et al.* 2015; Dong *et al.* 2020). The Early Cretaceous Liuqiong adakites (*c.* 140–137 Ma) reported in this work occur near the YZSZ. After excluding the above processes related to adakite genesis and considering the emplacement age of the Liuqiong adakite, which is consistent with the Neo-Tethys subduction time (Zhu *et al.* 2009), combined with its moderately positive $\epsilon_{Nd}(t)$ values and highly positive zircon $\epsilon_{Hf}(t)$ values, we propose that the Liuqiong adakite more likely formed by partial melting of the subducted oceanic slab.

To further determine the petrogenesis of the Liuqiong adakite, we show a variety of adakite discriminant plots. Compared with other adakites, slab-melting adakites have higher $Mg^{\#}$ values and lower Th contents and Th/Ce ratios (Zhu *et al.* 2009). In the SiO_2–$Mg^{\#}$ (Fig. 12a) and Th–Th/Ce (Fig. 12b) plots, all samples from the Liuqiong adakite plot in the area of slab-related adakites, also showing an arc-related affinity. Furthermore, the high contents of Cr (57.0–139.10 ppm) and Ni (22.2–47.63 ppm) for the Liuqiong adakite are similar to those from the Mamen adakite-like rocks (Zhu *et al.* 2009), which plot in the field of subduction-related adakites (Fig. 12c). The plot of Al_2O_3–K_2O/Na_2O (Fig. 12d) clearly shows that the Liuqiong adakite has a high content of Al_2O_3 and a low ratio of K_2O/Na_2O, which is also consistent with subduction-related adakites. This evidence contradicts the process of partial melting of the thickened lower crust. The relatively high, homogeneous zircon $\epsilon_{Hf}(t)$ values (Fig. 10) and whole-rock $\epsilon_{Nd}(t)$ values (+5.78 to +6.24) are consistent with those from Tethyan-related basalt (Mahoney *et al.* 1998) and suggest that the Liuqiong adakite source magmas mainly originated from the partial melting of the Tethyan subducted oceanic slab.

In summary, we propose here that the formation process of the Liuqiong adakite is related to the partial melting of the Neo-Tethyan oceanic slab.

6.c. Nature of the source region

The Liuqiong adakite exhibits considerably negative Nb–Ta anomalies, suggesting an affinity with magmas generated in a subduction-related tectonic setting (Kelemen *et al.* 2007). The values of Nb/U for the Liuqiong adakite vary from 2.51 to 2.68 (with an average of 2.61), which is between the values of fluid derived from the subduction zone (≈0.22) (Ayers, 1998) and those of subducted sediments (≈5.0) (Plank & Langmuir, 1998), demonstrating an affinity with the subduction-related setting. Studies have shown that both slab-derived fluids and subducted-sediment melts can cause important changes in the composition of subduction-related magmas (Zhu *et al.* 2009). In the Th/Zr–Nb/Zr plot (Fig. 13a), the Liuqiong adakite shows a trend of subduction-related fluid metasomatism, which implies the addition of subducting fluids to the genesis of these rocks. Subducted sediment melts have relatively high Th and Pb contents and low Ce/Th (≈8), Ce/Pb (≈3) and

https://doi.org/10.1017/S0016756822000401 Published online by Cambridge University Press

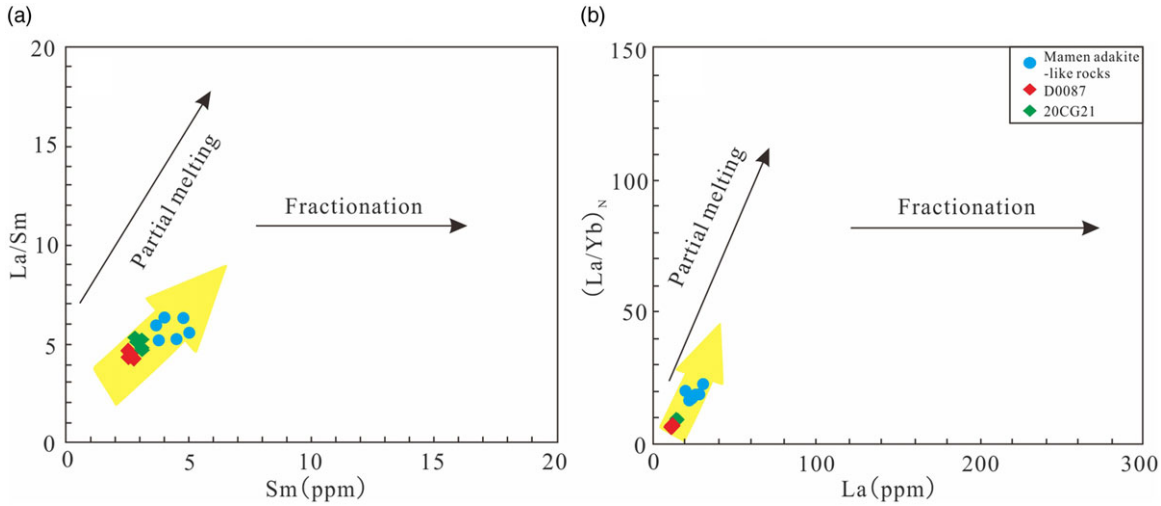

Fig. 11. (Colour online) Chemical variation plots of the Liuqiong adakite (after Long *et al.* 2015).

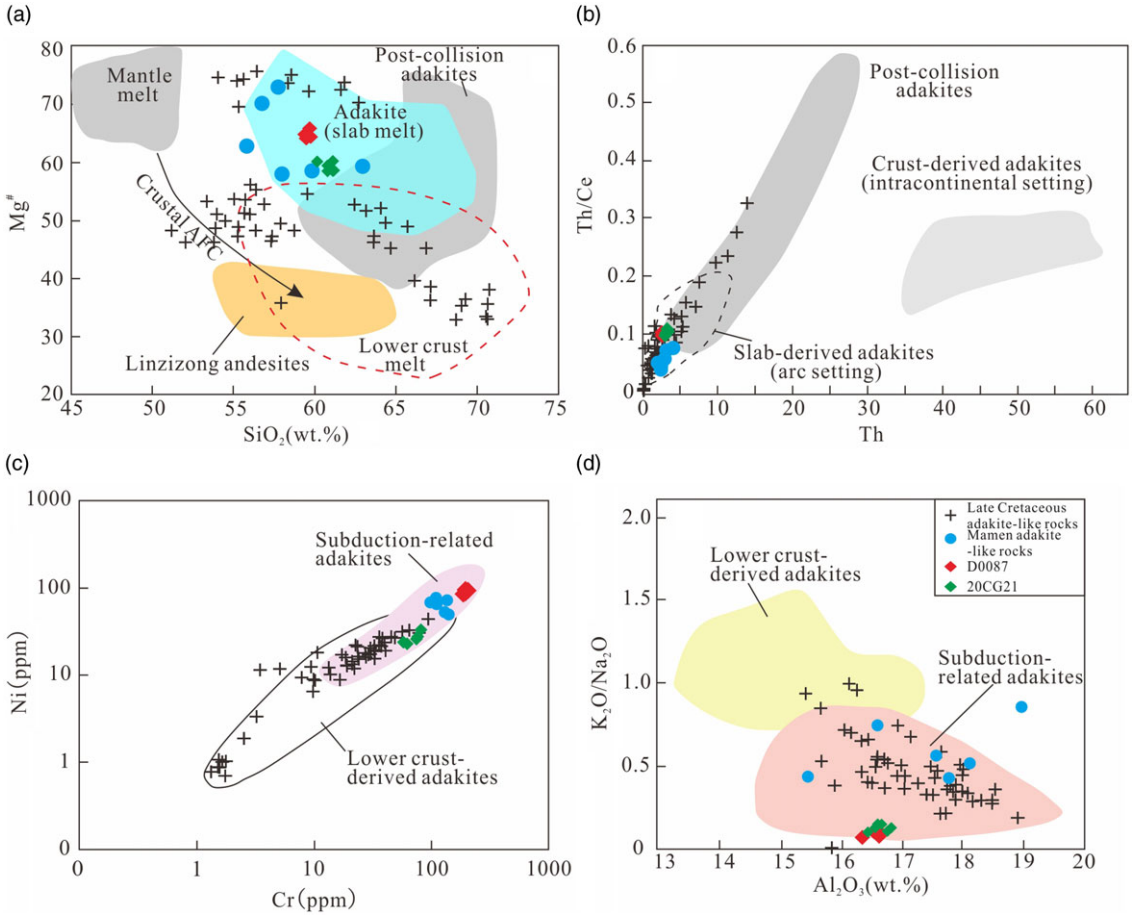

Fig. 12. (Colour online) Discrimination plots for the Liuqiong adakite. (a) $Mg^{\#}$–SiO_2 (after Zhu *et al.* 2009). (b) (Th/Ce)–Th (after Zhu *et al.* 2009). (c) Cr–Ni (after Guan *et al.* 2012). (d) (K_2O/Na_2O)–Al_2O_3 (after Jamshidi *et al.* 2018). Data are from the same source as in Fig. 6.

Ba/Th ratios (≈111) (Mao *et al.* 2014). The Ce/Th and Ce/Pb ratios of our samples range from 9.40 to 10.14 (with an average of 9.72) and from 1.08 to 5.42 (with an average of 2.93), respectively. In addition, the average Ba/Th value of the samples is 48. Based on the aforementioned ratios, we suggest that the source of the Liuqiong adakites also has a certain amount of sediment melt. In addition, Woodhead *et al.* (2001) proposed that the addition of sediment melt into the magma source may cause a significant increase in the Th/Yb ratio (>2). The Th/Yb values of the Liuqiong adakite are greater than 2, with an average of 2.41, reinforcing the addition of sediment melt in its magma source. The Th/Sm–Th/Yb plot (Fig. 13b) shows that Liuqiong samples

https://doi.org/10.1017/S0016756822000401 Published online by Cambridge University Press

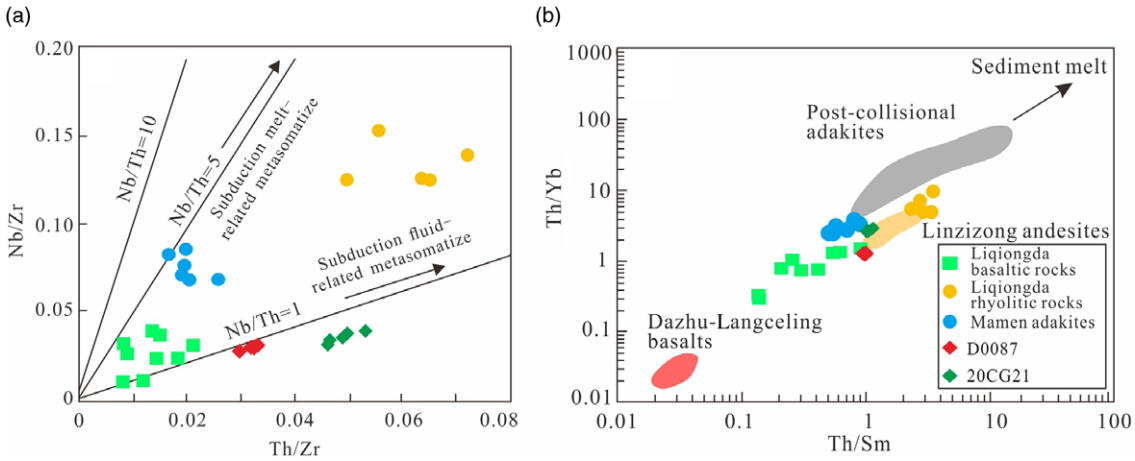

Fig. 13. (Colour online) Th/Zr – Nb/Zr plot (after Woodhead *et al.* 2001) (a) and Th/Sm–Th/Yb plot (after Zhu *et al.* 2009) (b) for the Liuqiong adakite.

have similar elemental compositions to those of the Mamen adakite-like rocks; both are considered a mixture between the Dazhu–Langceling basalts from the YZSZ and the partial melt of subducted sediment (Zhu *et al.* 2009).

Oceanic crust basalts and ocean–pelagic sediments have significantly different Sr and Nd isotope compositions. Therefore, subducted sediment melts not only cause a change in the trace elements of arc-related magmas but also leave a remarkable fingerprint on their isotope composition (Plank & Langmuir, 1998). A large amount of Sr and Nd isotope data enables quantification of the relative contribution of sediments to the arc magma associated with subduction. Accordingly, the Dazhu–Langceling basalts from the YZSZ (Zhang *et al.* 2005) and the Indian Ocean pelagic sediment (Ben Othman *et al.* 1989) are considered the normal mid-ocean ridge basalt (N-MORB) and Neo-Tethyan oceanic sediment source components, respectively. Thus, we can clearly determine from the $^{87}Sr/^{86}Sr_i$ versus $\epsilon_{Nd}(t)$ plot that the source magma of the Liuqiong adakite could be regarded as a mixture of Neo-Tethyan subducting sediments (*c.* 5–10 %) and Tethyan basalt (Fig. 14a). Furthermore, the Indian MORB, which probably represents newly formed oceanic crust, exhibits zircon $\epsilon_{Hf}(t)$ values consistent with those of the Liuqiong adakite (Fig. 14b) (Zhu *et al.* 2009). Of course, we note that the Sr isotope compositions of the sample have a small deviation from the modelled curve, and we believe that an alternative and reasonable explanation could be the previous interaction of the Tethyan oceanic crust with seawater, which could raise the Sr isotope composition of the oceanic floor basalts (Fig. 14a).

The subducted oceanic slab-derived adakite might be influenced by slight interaction with peridotite in the overlying mantle wedge during magma ascent (Zhu *et al.* 2009). Notably, the Cr, Ni and MgO contents of the Liuqiong adakite (with averages of 99 ppm, 35 ppm and 3.65 wt %, respectively) are higher than those of typical adakites (Defant *et al.* 1991). The experimental results show that during ascent through the mantle wedge, the contents of Cr, Ni and MgO increase significantly because of the metasomatic reactions within the overlying mantle wedge (Rapp *et al.* 1999). In the case of a low level of interaction with peridotite in the mantle wedge during magma ascent, the increase in the above-mentioned elements may not be significant enough (B Wang *et al.* 2021). Such an interpretation is enlightening for determining the evolution of the Liuqiong adakite, indicating that the Liuqiong adakite magma clearly interacted with peridotite in the mantle wedge during ascent.

The Liuqiong adakite magma was derived from the partial melting of the Neo-Tethyan oceanic slab (MORB + sediment + fluid) and interacted with peridotite in the mantle wedge during magma ascent.

6.d. Geodynamic implications

The subduction initiation of the Neo-Tethys has always a widely debated issue in geosciences and has been proposed, by many studies, to have occurred sometime from the Late Triassic to the Early Cretaceous (Ji *et al.* 2009; Zhu *et al.* 2011; Kang *et al.* 2014; Huang *et al.* 2015; Zhong *et al.* 2016; Meng *et al.* 2021; XH Wang *et al.* 2021); other scholars believe that the Neo-Tethys was still not subducting during the Early Cretaceous (Wu *et al.* 2016). With the affinities of subduction-related adakites, the Liuqiong quartz diorites reported in this work are closely related to the subduction of the Neo-Tethyan oceanic slab. The emplacement age of *c.* 141 Ma from our samples illustrates that the northward subduction of the Neo-Tethyan oceanic crust was already active prior to 141 Ma or even earlier.

The subduction pattern of the Neo-Tethys Ocean during the Early Cretaceous has also been debated in the literature. The prevalent viewpoints about the subduction model include flat-lying (low-angle) subduction (Coulon *et al.* 1986; Ding & Lai 2003; Kapp *et al.* 2005, 2007; Zhang *et al.* 2012; Wang *et al.* 2017), high-angle subduction (Zhu *et al.* 2009) and intra-ocean subduction (Aitchison *et al.* 2000; McDermid *et al.* 2002; Xu *et al.* 2009). Additionally, an oblique subduction setting has been proposed (Ji *et al.* 2009). Based on the available data, Early Cretaceous magmatism was widely distributed in the central and northern parts of the Lhasa terrane (Ding *et al.* 2003; Kapp *et al.* 2007). Although Early Cretaceous magmatism has been reported (Zhu *et al.* 2009; Wang *et al.* 2017), evidence of this magmatic activity is rare at the southern margin of the Lhasa terrane, which might not be attributed to stable oblique subduction (Gutscher *et al.* 2000).

Located near the sampling site of our study, the Liqiongda Early Cretaceous volcanic rocks were most likely produced in a typical active continental margin setting (Wang *et al.* 2017), which does not support the suggestion of intra-ocean subduction during the Early Cretaceous. The Cuocun gabbro in the southern Lhasa

https://doi.org/10.1017/S0016756822000401 Published online by Cambridge University Press

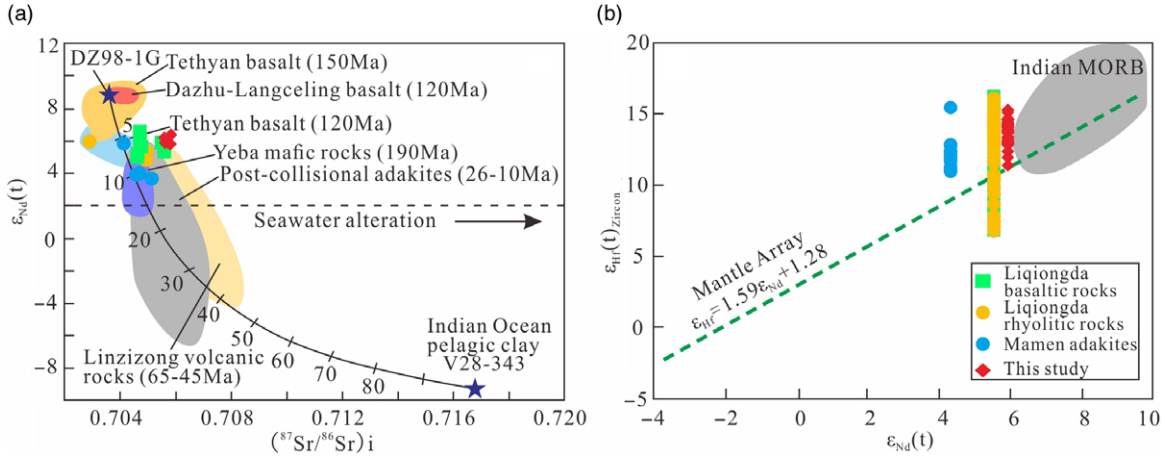

Fig. 14. (Colour online) $\epsilon_{Nd}(t)$–$(^{87}Sr/^{86}Sr)_i$ and $\epsilon_{Nd}(t)$–$\epsilon_{Hf}(t)$ plots for the Liuqiong adakite (after Zhu *et al.* 2009).

terrane also supports the conclusion that the Early Cretaceous magmatic rocks reassembled to a continental margin arc setting (He *et al.* 2020). Furthermore, previous studies have suggested that the Zedong terrane is a remnant of a Cretaceous intra-ocean subduction system in the southern margin of the Lhasa terrane (Aitchison *et al.* 2000). A subsequent study has show that the Zedong terrane formed in the Late Jurassic (McDermid *et al.* 2002) and is more likely to be a part of the Gangdese arc (Zhang *et al.* 2014). Recently, Liu *et al.* (2020) also suggested that the Zedong ophiolite, which may represent an intra-oceanic arc system, formed in the Late Jurassic. We can thus consider that models of intra-ocean subduction and stable oblique subduction are not suitable for explaining the evolution of the Neo-Tethys during the Early Cretaceous.

Different angles of oceanic slab subduction will produce different effects in the overlying plate. Normally, the contact surface between a low-angle (flat-lying) subducting oceanic plate and the overlying plate is large; in this case, the coupling between the two plates is tight, so the corresponding arc magmatism is relatively scarce. The overlying plate is strongly compressed and is the locus of significant orogeny (Yan *et al.* 2020). Therefore, the lull of arc magmatism and landward migration and the deformation of the overlying plate are important geological bases for recognizing (or proposing) the low-angle subduction of oceanic crust. Based on comprehensive regional data, the Mesozoic magma activities within the Gangdese arc shifted from south to north, showing a trend of landward migration (Wang *et al.* 2017); they may be the response to the location of the front part of the flat-lying Neo-Tethyan oceanic slab (Dai, 2012). Specifically, volcanic activity migrated northwards in response to the shallowing of the subduction angle of the downgoing Neo-Tethyan slab from the latest Jurassic through the Early Cretaceous (Coulon *et al.* 1986; Kapp *et al.* 2005; Leier *et al.* 2007). In addition, many leucogranites within the Gangdese batholith record the thickening of the crust and mountain-building process, which is the response of the northward Neo-Tethyan subduction during the Early Cretaceous (~140–130 Ma) (Ding & Lai, 2003). From our study data, we conclude that the subduction of the Neo-Tethys began before the Early Cretaceous (~141 Ma). Stratigraphic data indicate the uplift and deformation of the Lhasa terrane in the Early Cretaceous (Leier *et al.* 2007). We favour the interpretation that the Neo-Tethyan oceanic crust was subducted beneath the Lhasa terrane at a low angle during the Early Cretaceous.

The discovery of Mamen adakite-like rocks (~137 Ma) and contemporary volcanic rocks (~130 Ma; Zhu *et al.* 2008) in the study region has prompted some researchers to support the model of high-angle subduction of the Neo-Tethyan oceanic crust (Zhu *et al.* 2009). Considering that there is no report of large-scale, Early Cretaceous magma on the southern margin of the Gangdese batholith, we believe that the high-angle subduction model may not be appropriate. Adakites form under high temperatures (above 700 °C), even corresponding to a relatively shallow subducted-slab angle (Gutscher *et al.* 2000), which may account for the sporadic Early Cretaceous adakites in the southern margin of the Lhasa terrane. Systematic temperature changes are revealed by variations in zircon Ti content. The Ti contents of the investigated Liuqiong quartz diorite zircons vary from 1.88 to 7.00 ppm. According to the crystallization thermometer for zircon (Watson *et al.* 2006), we can infer that the average crystallization temperature of these zircons is 745 °C. Considering the crystallization process of minerals in the magma system, the zircon crystallization temperature could serve as the lower temperature of melting originating from the subducted oceanic slabs. Hence, the partial melting temperature should be higher than the temperature obtained by the zircon Ti thermometer (CW Li *et al.* 2020). Therefore, the partial melting temperature to form the Liuqiong adakite melt should be higher than ~745 °C, reaching the temperature conditions for adakite formation considered by previous studies (Gutscher *et al.* 2000).

Recent geological survey reveals that the ages of accretionary complexes gradually become younger from the Tangjia–Sumdo area in the north, to the Yarlung–Zangbo River in the south (GM Li *et al.* 2020), for example, the Permian – Middle Triassic ($P–T_2$) accretionary complex, Late Triassic – Early Jurassic ($T_3–J_1$) accretionary complex (Fig. 15) and Cretaceous ($K_{1–2}$) accretionary complex (unpublished data), from north to south. Therefore, some studies consider that continuous southward accretion took place at the SE margin of Gangdese after the Late Palaeozoic and that the Tangjia–Sumdo Palaeo-Tethys and the Neo-Tethys might represent different evolutionary phases of the same ocean (GM Li *et al.* 2020; Xie *et al.* 2020). Recent studies have identified numerous Jurassic granites in the Sumdo area, which are attributed

https://doi.org/10.1017/S0016756822000401 Published online by Cambridge University Press

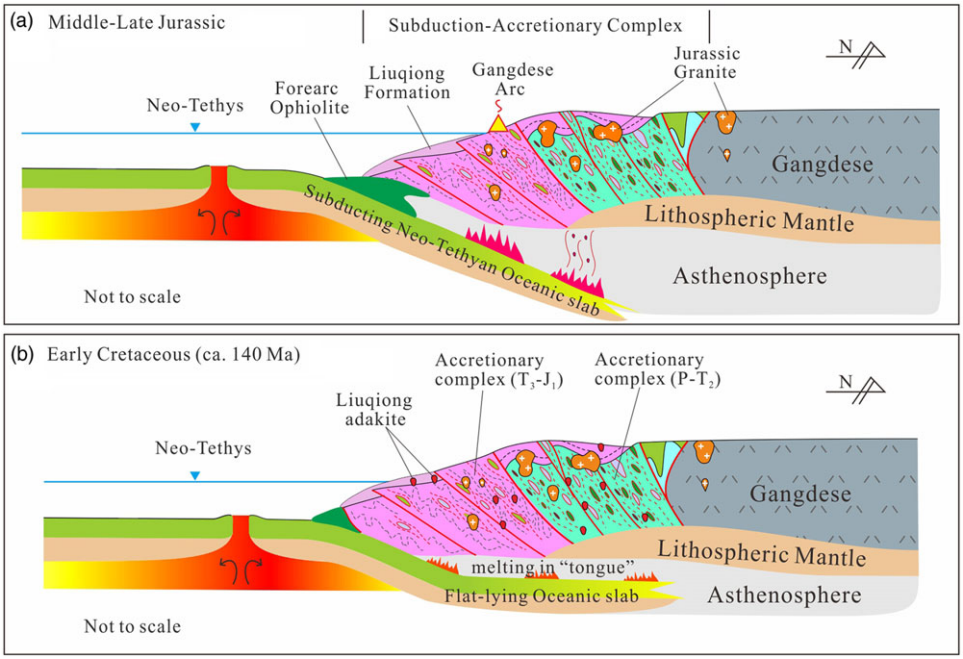

Fig. 15. (Colour online) Schematic tectonic evolution models of the SE margin of Gangdese. (a) Normal oblique subduction of the Neo-Tethys Ocean during the Middle–Late Jurassic. (b) Flat-slab subduction of the Neo-Tethyan oceanic slab and the generation of the Liuqiong adakite in the Early Cretaceous. More details are provided in the text.

to remelting of the crust caused by the underlying mass of mantle-derived material (Song *et al.* 2022), and suggest that the Neo-Tethyan oceanic plate was not in a state of flat-slab subduction in the Jurassic (since the upwelling of large amounts of mantle-derived material could not be achieved during flat-slab subduction). In addition, volcanic rocks of the Yeba Formation (YBF) (~183–174 Ma) suggest a back-arc extensional setting for the Early–Middle Jurassic (Wei *et al.* 2017). These studies indicate that the Neo-Tethys Ocean subducted at a normal angle in the Jurassic. Moreover, fore-arc extension produced ophiolite in the Zedang area during the period 160–150 Ma (Liu *et al.* 2020; Dai *et al.* 2021), also demonstrating that the Neo-Tethys Ocean did not enter the stage of flat-slab subduction at this time (Fig. 15a). In our study, the Liuqiong adakite magma (~140 Ma) shows some degree of peridotite interaction within the overlying mantle wedge. Considering the above studies, we believe that the Neo-Tethys Ocean was most likely formed during this stage (*c.* 140 Ma), transitioning to a flat-slab setting soon after but maintaining a tongue-shaped mantle wedge to account for the peridotite interaction during magma ascent, which may account for the slight interaction with the tongue-shaped mantle wedge (Fig. 15b). Subsequently, the mantle wedge disappeared, and magmatism ceased, especially during the period between 137 and 120 Ma in the study area. The latest evidence of ocean subduction-related magmatic rocks was found in upper Lower Cretaceous (~120–112 Ma) strata in the Zedang Trench basin in the form of detrital zircons (Y Zhong, unpublished data).

Nevertheless, the classical flat-slab subduction model predicts a 'wide adakitic magma arc', whereas a narrow calc-alkaline arc (volcanic line) is predicted in the normal situation (Gutscher *et al.* 2000). The sporadic Early Cretaceous rocks in the southern margin of the Lhasa terrane are not compatible with a steeply dipping Neo-Tethyan slab. In our proposed tectonic model, we emphasize a tongue-shaped mantle wedge during the Early Cretaceous (Fig. 15b), and we interpret the slight interaction with the mantle wedge from this finding. Additionally, because of the tongue-shaped mantle wedge, the magmatism caused by flat-slab subduction would have been small-scale, which is not widely reported for normal arc magmatic rocks. Although a 'wide magma arc' is predicted by Gutscher *et al.* (2000), we may consider that this limited magmatism resulted in only small-scale intrusive rocks. For example, the flat subduction of the Palaeo-Pacific Plate during the Middle Triassic produced localized granitic intrusions in South China (Zhang *et al.* 2021).

Consequently, we conclude that the sporadic Early Cretaceous adakites at the southern margin of the Lhasa terrane were triggered by low-angle subduction of the Neo-Tethyan oceanic lithosphere.

7. Conclusions

(1) LA-ICP-MS zircon U–Pb dating indicates that the porphyritic Liuqiong quartz diorite was emplaced *c.* 141-137 Ma, providing evidence for Early Cretaceous magmatism along the southern margin of the Lhasa terrane.
(2) Liuqiong quartz diorite has high contents of SiO_2, Al_2O_3 and Sr, in combination with low concentrations of HREEs and Y, which is similar to the geochemical signature of typical adakites.
(3) The Liuqiong adakite was probably derived from the partial melting of the subducted Neo-Tethyan slab (MORB + sediment + fluid) and the subsequent interaction with mantle peridotite within the overlying mantle wedge.
(4) We favour the viewpoint that the Neo-Tethyan oceanic lithosphere was flat-lying beneath the Lhasa terrane during the Early Cretaceous.

Supplementary material. To view supplementary material for this article, please visit https://doi.org/10.1017/S0016756822000401

Acknowledgements. We thank Bo Li, Junge Qin, Yuanyin Jia, Tengxiao Ma and Zhichao Cao for their assistance in writing. We also thank the editor and two anonymous reviewers for their handling of the manuscript and constructive comments. This study was supported financially by the National Natural Science Foundation of China (Grant No. 41972118) and the Gangdese-

Himalayan Copper Resource Base Investigation Project (Grant No. DD20160015).

Conflict of interest. The authors declare that they have no known competing financial interests or personal relationships that could have appeared to influence the work reported in this paper.

References

Aitchison JC, Badengzhu Davis AM, Liu JB, Luo H, Malpas JG, McDermid IRC, Wu HY, Ziabrev SV and Zhou MF (2000) Remnants of a Cretaceous intra-oceanic subduction system within the Yarlung–Zangbo suture (southern Tibet). *Earth and Planetary Science Letters* **183**, 231–44.

Allègre CJ, Courtillot V and Tapponnier P (1984) Structure and evolution of the Himalaya–Tibet orogenic belt. *Nature* **307**, 17–22.

Amelin Y, Lee DC, Halliday AN and Pidgeon RT (1999) Nature of the Earth's earliest crust from hafnium isotopes in single detrital zircons. *Nature* **399**, 1497–503.

Andersen T (2002) Correction of common lead in U–Pb analyses that do not report ^{204}Pb. *Chemical Geology* **192**, 59–79.

Atherton MP and Petford N (1993) Generation of sodium-rich magmas from newly under-plated basaltic crust. *Nature* **362**, 144–6.

Ayers J (1998) Trace element modeling of aqueous fluid–peridotite interaction in the mantle wedge of subduction zones. *Contributions to Mineralogy and Petrology* **132**, 390–404.

Bédard É, Hébert R, Guilmette C, Lesage G, Wang CS and Dostal J (2009) Petrology and geochemistry of the Saga and Sangsang ophiolitic massifs, Yarlung-Zangbo Suture Zone, Southern Tibet: evidence for an arc–back-arc origin. *Lithos* **113**, 48–67.

Belousova E, Griffin W, O'Reilly SY and Fisher N (2002) Igneous zircon: trace element composition as an indicator of source rock type. *Contributions to Mineralogy and Petrology* **143**, 602–22.

Ben Othman D, White WM and Patchett J (1989) The geochemistry of marine sediments, island arc magma genesis and crust–mantle recycling. *Earth and Planetary Science Letters* **94**, 1–21.

Castillo PR, Janney PE and Solidum R (1999) Petrology and geochemistry of Camiguin Island, southern Philippines: insights into the source of adakite and other lavas in a complex arc tectonic setting. *Contributions to Mineralogy and Petrology* **134**, 33–51.

Chen YH, Yang JS, Xiong FH, Zhang L, Lai SM and Chen M (2015) Geochronology and geochemistry of the subduction-related rocks with high Sr/Y ratios in the Zedong area: implications for the magmatism in southern Lhasa terrane during Late Cretaceous. *Acta Geologica Sinica (English Edition)* **89**, 351–68.

Chu MF, Chung SL, Song B, Liu DY, O'Reilly SY and Pearson NJ (2006) Zircon U-Pb and Hf isotope constraints on the Mesozoic tectonics and crustal evolution of Southern Tibet. *Geology* **34**, 745–8.

Chung SL, Liu DY, Ji JQ, Chu MF, Lee HY, Wen DJ, Lo CH, Lee TY, Qian Q and Zhang Q (2003) Adakites from continental collision zones: melting of thickened lower crust beneath southern Tibet. *Geology* **31**, 1021–4.

Condie KC (2005) TTGs and adakites: are they both slab melts? *Lithos* **80**, 33–44.

Coulon C, Maluski H, Bollinger C and Wang S (1986) Mesozoic and Cenozoic volcanic rocks from central and southern Tibet: ^{39}Ar/^{40}Ar dating, petrological characteristics and geodynamical significance. *Earth and Planetary Science Letters* **79**, 281–302.

Dai JG (2012) *Research on several key question of Yarlung-Zangbo Ophiolite Zone, Tibet and its adjacent area*. PhD thesis, China University of Geosciences. Wuhan. Published thesis (in Chinese with English abstract).

Dai JG, Wang CS, Stern RJ, Yang K and Shen J (2021) Forearc magmatic evolution during subduction initiation: insights from an Early Cretaceous Tibetan ophiolite and comparison with the Izu-Bonin-Mariana forearc. *Geological Society of America Bulletin* **133**, 753–76.

Dai ZW, Li GM, Ding J, Huang Y and Cao HW (2018) Late Cretaceous adakite in Nuri area, Tibet: products of ridge subduction. *Earth Science* **43**, 2727–41 (in Chinese with English abstract).

Defant MJ and Drummond MS (1990) Derivation of some modern arc magmas by melting of young subducted lithosphere. *Nature* **347**, 662–5.

Defant MJ, Richerson PM, de Boer JZ, Stewart RH, Maury RC, Bellon H, Drummond MS, Feigenson MD and Jackson TE (1991) Dacite genesis via both differentiation and slab melting: petrogenesis of La Yeguada volcanic complex, Panama. *Journal of Petrology* **32**, 1101–42.

Dewey JF (2005) Orogeny can be very short. *Proceedings of the National Academy of Sciences, USA (PNAS)* **102**, 15286–93.

Ding L, Kapp P, Zhong DL and Deng WM (2003) Cenozoic volcanism in Tibet: evidence for a transition from oceanic to continental subduction. *Journal of Petrology* **44**, 1833–65.

Ding L and Lai QZ (2003) New geological evidence of crustal thickening in the Gangdese block prior to the Indo-Asian collision. *Chinese Science Bulletin* **48**, 1604–10.

Dong YC, Wang M, Xie CM, Yu YP and Hao YJ (2020) Genesis and tectonic indication of the Late Cretaceous adakite rocks in the Lamunale area, Nima County, Tibet. *Acta Petrologica Sinica* **36**, 426–42 (in Chinese with English abstract).

Gao J, Klemd R, Long LL, Xiong XM and Qian Q (2009) Adakitic signature formed by fractional crystallization: an interpretation for the neo-Proterozoic meta-plagiogranites of the NE Jiangxi ophiolitic mélange belt, South China. *Lithos* **110**, 277–93.

Guan Q, Zhu DC, Zhao ZD, Dong GC, Zhang LL, Li WX, Liu M, Mo XX, Liu YS and Yuan HL (2012) Crustal thickening prior to 38 Ma in southern Tibet: evidence from lower crust-derived adakitic magmatism in the Gangdese Batholith. *Gondwana Research* **21**, 88–99.

Guan Q, Zhu DC, Zhao ZD, Zhang LL, Liu M, Li WX, Yu F and Mo XX (2010) Late Cretaceous adakites in the eastern segment of the Gangdese Belt, southern Tibet: products of Neo-Tethyan ridge subduction?. *Acta Petrologica Sinica* **26**, 2165–79 (in Chinese with English abstract).

Guo F, Nakamuru E, Fan W, Kobayoshi K and Li C (2007) Generation of Palaeocene adakitic andesites by magma mixing; Yanji area, NE China. *Journal of Petrology* **48**, 661–92.

Guo Z, Wilson M and Liu J (2007) Post-collisional adakites in south Tibet: products of partial melting of subduction-modified lower crust. *Lithos* **96**, 205–24.

Gutscher MA, Maury R, Eissen JP and Bourdon E (2000) Can slab melting be caused by flat subduction?. *Geology* **28**, 535–8.

He Q, Lang XH, Li Liang, Chen CH, Wang XH, Deng YL, Yin Q, Xie FW, Yang ZY and Zhang Z (2020) U-Pb zircon age and geochemistry of the Cuocun gabbro in the southern Lhasa terrane: implications for Early Cretaceous rollback of the Neo-Tethyan oceanic slab. *Geological Journal* **56**, 1424–44.

Hoskin PWO and Black LP (2010) Metamorphic zircon formation by solid-state recrystallization of protolith igneous zircon. *Journal of Metamorphic Geology* **18**, 423–39.

Hou KJ, Li YH, Zou TR, Qu XM, Shi YR and Xie GQ (2007) Laser Ablation-MC-ICP-MS technique for Hf isotope microanalysis of zircon and its geological applications. *Acta Petrologica Sinica* **23**, 2595–604 (in Chinese with English abstract).

Hou ZQ, Gao YF, Qu XM, Rui ZY and Mo XX (2004) Origin of adakitic intrusives generated during Mid-Miocene east–west extension in southern Tibet. *Earth and Planetary Science Letters* **220**, 139–55.

Huang F, Xu JF, Chen JL, Kang ZQ and Dong YH (2015) Early Jurassic volcanic rocks from the Yeba Formation and Sangri Group: products of continental marginal arc and intra-oceanic arc during the subduction of Neo-Tethys Ocean? *Acta Petrologica Sinica* **31**, 2089–100 (in Chinese with English abstract).

Jamshidi D, Ghasemi H, Miao LC and Sadeghian M (2018) Adakite magmatism within the Sabzevar ophiolite zone, NE Iran: U-Pb geochronology and Sr-Nd isotopic evidences. *Geopersia* **8**, 111–30.

Ji WQ, Wu FY, Chung SL, Li JX and Liu CZ (2009) Zircon U-Pb geochronology and Hf isotopic constraints on petrogenesis of the Gangdese batholith, southern Tibet. *Chemical Geology* **262**, 229–45.

Kang ZQ, Xu JF, Chen JL and Wang BD (2009) Geochemistry and origin of Cretaceous adakites in Mamuxia Formation, Sangri Group, South Tibet. *Geochimica* **38**, 334–44.

Kang ZQ, Xu JF, Wilde SA, Feng ZH, Chen JL, Wang BD, Fu WC and Pan HB (2014) Geochronology and geochemistry of the Sangri Group volcanic

rocks, southern Lhasa terrane: implications for the early subduction history of the Neo-Tethys and Gangdese magmatic arc. *Lithos* **200–201**, 157–68.

Kapp P, Decelles PG, Gehrels GE, Heizler M and Ding L (2007) Geological records of the Lhasa-Qiangtang and Indo-Asian collisions in the Nima area of Central Tibet. *Geological Society of America Bulletin* **119**, 917–32.

Kapp P, Yin A, Harrison TM and Ding L (2005) Cretaceous-Tertiary shortening, basin development, and volcanism in central Tibet. *Geological Society of America Bulletin* **117**, 865–78.

Kelemen PB, Hanghoj K and Greene AR (2007) One view of the geochemistry of subduction-related magmatic arcs, with an emphasis on primitive andesite and lower crust. *Treatise on Geochemistry* **138**, 1–70.

Lai SC and Qin JF (2013) Adakitic rocks derived from the partial melting of subducted continental crust: evidence from the Eocene volcanic rocks in the northern Qiangtang Block. *Gondwana Research* **23**, 812–24.

Leier AL, Decelles PG, Kapp P and Gehrels GE (2007) Lower Cretaceous strata in the Lhasa terrane, Tibet, with implications for understanding the early tectonic history of the Tibetan Plateau. *Journal of Sedimentary Research* **77**, 809–25.

Li CW, Zeng M, Li ZJ and Chen S (2020) Origin and tectonic implications of Late Jurassic high-Mg diorites along the Bangong-Nujiang suture zone, Tibet. *International Geology Review* **8**, 1–17.

Li GM, Zhang LK, Wu JY, Xie CM, Zhu LD and Han FL (2020) Reestablishment and scientific significance of the ocean plate geology in the southern Tibet Plateau, China. *Sedimentary Geology and Tethyan Geology* **40**, 1–14 (in Chinese with English abstract).

Liu WL, Zhong Y, Sun ZL, Yakymchuk C, Gu M, Tang GJ, Zhong LF, Cao H, Liu HF and Xia B (2020) The Late Jurassic Zedong ophiolite: a remnant of subduction initiation within the Yarlung Zangbo Suture Zone (southern Tibet) and its tectonic implications. *Gondwana Research* **78**, 172–88.

Long XP, Wilde SA, Wang Q, Yuan C, Wang XC, Li J, Jiang ZQ and Dan W (2015) Partial melting of thickened continental crust in central Tibet: evidence from geochemistry and geochronology of Eocene adakitic rhyolites in the northern Qiangtang terrane. *Earth and Planetary Science Letters* **414**, 30–44.

Lu TY, He ZY and Klemd R (2020) Two phases of post-onset collision adakitic magmatism in the southern Lhasa subterrane, Tibet, and their tectonic implications. *Geological Society of America Bulletin* **132**, 1587–602.

Ludwig KR (2003) *User's Manual for Isoplot 3.00: A Geochronological Toolkit for Microsoft Excel*. Berkeley, California: Berkeley Geochronology Center Special Publication, 70 pp.

Ma L, Wang Q, Wyman DA, Li ZX, Jiang ZQ, Yang JH, Gou GN and Guo HF (2013) Late Cretaceous (100-89 Ma) magnesian charnockites with adakitic affinities in the Milin area, eastern Gangdese: partial melting of subducted oceanic crust and implications for crustal growth in southern Tibet. *Lithos* **175–176**, 315–32.

Mahoney JJ, Frei R, Tejada MLG, Mo XX, Leat PT and Nägler TF (1998) Tracing the Indian Ocean Mantle Domain through time: isotopic results from Old West Indian, East Tethyan, and South Pacific Seafloor. *Journal of Petrology* **39**, 1285–306.

Mao QG, Wang JB, Xiao WJ, Fang TH, Wang N and Yu MJ (2014) The discovery of Low-Carboniferous arc volcanic rocks and its tectonic significance at the Kalatage area in the central Tianshan, eatern Tianshan Mountains, Xinjiang, NW China. *Acta Geologica Sinica* **88**, 1790–9 (in Chinese with English abstract).

McDermid I, Aitchison J, Davis A, Harrison T and Grove M (2002) The Zedong terrane: a Late Jurassic intra-oceanic magmatic arc within the Yarlung-Zangbo Suture Zone, southeastern Tibet. *Chemical Geology* **187**, 267–77.

Meng YK, Mooney WD, Fan RL, Liu JQ and Wei YQ (2021) Identification of the Early Jurassic mylonitic granitic pluton and tectonic implications in Namling area, southern Tibet. *Geoscience Frontiers* **12**, 13–28.

Middelburg JJ, Weijden C and Woittiez J (1988) Chemical processes affecting the mobility of major, minor and trace elements during weathering of granitic rocks. *Chemical Geology* **68**, 253–73.

Middlemost E (1994) Naming materials in the magma/igneous rock system. *Earth Science Reviews* **37**, 215–24.

Najman Y, Jenks D, Godin L, Boudagher-Fadel M, Millar I, Garzanti E, Horstwood M and Bracciali L (2017) The Tethyan Himalayan detrital record shows that India-Asia terminal collision occurred by 54 Ma in the western Himalaya. *Earth and Planetary Science Letters* **459**, 301–10.

Pan GT, Mo XX, Hou ZQ, Zhu DC, Wang LQ, Li GM, Zhao ZD, Geng QR and Liao ZL (2006) Spatial-temporal framework of the Gangdese Orogenic Belt and its evolution. *Acta Petrologica Sinica* **22**, 521–33 (in Chinese with English abstract).

Plank T and Langmuir CH (1998) The chemical composition of subducting sediment and its consequences for the crust and mantle. *Chemical Geology* **145**, 325–94.

Polat A and Hofmann AW (2003) Alteration and geochemical patterns in the 3.7–3.8 Ga Isua greenstone belt, West Greenland. *Precambrian Research* **126**, 197–218.

Rapp RP, Shimizu N, Norman MD and Applegate GS (1999) Reaction between slab-derived melts and peridotite in the mantle wedge: experimental constraints at 3.8 GPa. *Chemical Geology* **160**, 335–56.

Rollinson HR (1993) *Using Geochemical Data: Evaluation, Presentation, Interpretation*. London: Longman Group UK Ltd, 352 pp.

Shahbazi H, Taheri, Maghami Y, Azizi H, Asahara Y, Siebel W, Maanijou M and Rezai A (2021) Zircon U–Pb ages and petrogenesis of late Miocene adakitic rocks from the Sari Gunay gold deposit, NW Iran. *Geological Magazine* **158**, 1733–5.

Song YH, Xie CM, Gao ZW, Yu YP, Wang B, Duan ML and Hao YJ (2022) Tectonic transition from Paleo- to Neo-Tethyan Ocean in Tangjia-Sumdo area, Southern Tibet: constraints from Early Jurassic magmatism. *Gondwana Research* **105**, 12–24.

Stern CR and Kilian R (1996) Role of the subducted slab, mantle wedge and continental crust in the generation of adakites from the Andean Austral Volcanic Zone. *Contributions to Mineralogy and Petrology* **123**, 263–81.

Stern RJ (2002) Subduction zones. *Reviews of Geophysics* **40**, 1012.

Streck MJ, Leeman WP and Chesley J (2007) High-magnesian andesite from Mount Shasta: a product of magma mixing and contamination, not a primitive mantle melt. *Geology* **35**, 351–4.

Sun SS and McDonough WF (1989) Chemical and isotopic systematics of oceanic basalts: implications for mantle composition and processes. In *Magmatism in the Oceanic Basins* (eds AD Saunders & MJ Norry), pp. 313–45. *Geological Society of London, Special Publication* **no. 42**.

Thompson J, Meffre S and Danyushevsky L (2018) Impact of air, laser pulse width and fluence on U-Pb dating of zircons by LA-ICP-MS. *Journal of Analytical Atomic Spectrometry* **33**, 221–30.

Wang B, Xie CM, Dong YS, Fan JJ, Yu YO and Duan ML (2021) Middle Permian adakitic granite dikes in the Sumdo region, central Lhasa terrane, central Tibet: implications for the subduction of the Sumdo Paleo-Tethys ocean. *Journal of Asian Earth Sciences* **205**, 104610.

Wang C, Ding L, Liu ZC, Zhang LY and Yue YH (2017) Early Cretaceous bimodal volcanic rocks in the southern Lhasa terrane, south Tibet: age, petrogenesis and tectonic implications. *Lithos* **268**, 260–73.

Wang C, Ding L, Zhang LY, Kapp P, Pullen A and Yue YH (2016) Petrogenesis of Middle–Late Triassic volcanic rocks from the Gangdese belt, southern Lhasa terrane: implications for early subduction of Neo-Tethyan oceanic lithosphere. *Lithos* **262**, 320–33.

Wang Q, McDermott F, Xu JF, Bellon H and Zhu YT (2005) Cenozoic K-rich adakitic volcanic rocks in the Hohxil area, northern Tibet: lower-crustal melting in an intra-continental setting. *Geology* **33**, 465–8.

Wang Q, Wyman DA, Xu J, Jian P, Zhao Z, Li C, Xu W, Ma J and He B (2007) Early Cretaceous adakitic granites in the Northern Dabie Complex, central China: implications for partial melting and delamination of thickened lower crust. *Geochimica et Cosmochimica Acta* **71**, 2609–36.

Wang Q, Xu JF, Jian P, Bao ZW, Zhao ZH, Li CF, Xiong XL and Ma JL (2006) Petrogenesis of adakitic porphyries in an extensional tectonic setting, Dexing, south China: implications for the genesis of porphyry copper mineralization. *Journal of Petrology* **47**, 119–44.

Wang W, Zhai QG, Hu PY, Chung SL, Tang Y, Wang HT, Zhu ZC, Wu H and Huang ZQ (2020) Late Cretaceous adakitic rocks from the western Tibetan Plateau: implications for the subduction of the Neo-Tethys Ocean. *International Geology Review* **4**, 1–16.

Wang XH, Lang XH, Klemd R, Deng YL and Tang JX (2021) Subduction initiation of the Neo-Tethys oceanic lithosphere by collision-induced

https://doi.org/10.1017/S0016756822000401 Published online by Cambridge University Press

subduction transference. *Gondwana Research* **104**, 54–69. doi: 10.1016/j.gr.2021.08.012.

Watson EB, Wark DA and Thomas JB (2006) Crystallization thermometers for zircon and rutile. *Contributions to Mineralogy and Petrology* **151**, 413–33.

Wei YQ, Zhao ZD, Niu YL, Zhu DC, Liu D, Wang Q, Hou ZQ, Mo XX and Wei JC (2017) Geochronology and geochemistry of the Early Jurassic Yeba Formation volcanic rocks in southern Tibet: initiation of back-arc rifting and crustal accretion in the southern Lhasa Terrane. *Lithos* **278–281**, 477–90.

Wen DR, Chung SL, Song B, Iizuka Y, Yang HJ, Ji JQ, Liu DY and Galleta S (2008) Late Cretaceous Gangdese intrusions of adakitic geochemical characteristics, SE Tibet: petrogenesis and tectonic implications. *Lithos* **105**, 1–11.

Woodhead JD, Hergt JM, Davidson JP and Eggins SM (2001) Hafnium isotope evidence for 'conservative' element mobility during subduction zone processes. *Earth and Planetary Science Letters* **192**, 331–46.

Wu FY, Li XH, Zheng YF and Gao S (2007) Lu-Hf isotopic systematics and their applications in petrology. *Acta Petrologica Sinica* **23**, 185–220 (in Chinese with English abstract).

Wu FY, Yang YH, Xie LW, Yang JH and Ping X (2006) Hf isotopic compositions of the standard zircons and baddeleyites used in U–Pb geochronology. *Chemical Geology* **234**, 105–26.

Wu ZH, Zhao Z, Barosh PJ and Ye PS (2016) Early Cretaceous tectonics and evolution of the Tibetan Plateau. *Acta Geologica Sinica (English Edition)* **90**, 847–57.

Xie CM, Li C, Li GM, Zhang LK, Wang B, Dong YC and Hao YJ (2020) The research progress and problem of the Sumdo Paleo-Tethys Ocean, Tibet. *Sedimentary Geology and Tethyan Geology* **40**, 1–13 (in Chinese with English abstract).

Xu RK, Zheng YY, Feng QL, Shan L, Wei JH, Zhang X, Zhang GY, Ma GT and Pang YC (2009) Radiolarian chert and island-arc volcanic rocks in Xiapugou Tibet: records of Neo-Tethys intra-oceanic subduction system?. *Earth Science – Journal of China University of Geosciences* **34**, 884–94 (in Chinese with English abstract).

Xu WC, Zhang HF, Luo BJ, Guo L and Yang H (2015) Adakite-like geochemical signature produced by amphibole-dominated fractionation of arc magmas: an example from the Late Cretaceous magmatism in Gangdese Belt, south Tibet. *Lithos* **232**, 197–210.

Xu ZQ, Yang JS, Li HB, Zhang JX, Zeng LS and Jiang M (2006) The Qinghai-Tibet Plateau and continental dynamics: a review on terrain tectonics, collisional orogenesis, and processes and mechanisms for the rise of the plateau. *Geology in China* **33**, 221–38 (in Chinese with English abstract).

Yan ZY, Chen L, Xiong X, Wang K, Xie RX and Xu HZ (2020) Observations and modeling of flat subduction and its geological effects. *Science China Earth Sciences* **63**, 1069–91 (in Chinese with English abstract).

Yang YH, Zhang HF, Wu FY, Xie LW and Zhang YB (2005) Accurate measurement of strontium isotopic composition by Neptune Multiple Collector Inductively Coupled Plasma Mass Spectrometry. *Journal of Chinese Mass Spectrometry Society* **26**, 215–21 (in Chinese with English abstract).

Yao P, Li JG, Wang QH, Gu XX, Tang JX and Hui L (2006) Discovery and geological significance of the adakite in Gangdese island arc belt, Xizang (Tibet). *Acta Petrologica Sinica* **22**, 612–20 (in Chinese with English abstract).

Yin A and Harrison TM (2000) Geologic evolution of the Himalayan–Tibetan orogen. *Annual Review of Earth and Planetary Sciences* **28**, 211–80.

Zhang KJ, Zhang YX, Tang XC and Xia B (2012) Late Mesozoic tectonic evolution and growth of the Tibetan Plateau prior to the Indo-Asian collision. *Earth Science Reviews* **114**, 236–49.

Zhang LL, Liu CZ, Wu FY, Ji WQ and Wang JG (2014) Zedong terrane revisited: an intra-oceanic arc within Neo-Tethys or a part of the Asian active continental margin? *Journal of Asian Earth Sciences* **80**, 34–55.

Zhang Q, Wang Y, Liu W and Wang YL (2002) Adakite: its characteristics and implications. *Geological Bulletin of China* **21**, 431–5 (in Chinese with English abstract).

Zhang SQ, Mahoney JJ, Mo XX, Ghazi AM, Milani L, Crawford AJ, Guo TY and Zhao ZD (2005) Evidence for a widespread Tethyan upper mantle with Indian-Ocean-type isotopic characteristics. *Journal of Petrology* **46**, 829–58.

Zhang W, Zhang FQ, Dilek Y, Zhu KY, Wu HX, Chen DX and Chen HL (2021) Basin response to the Jurassic geodynamic turnover from flat subduction to normal subduction in South China. *Geological Society of America Bulletin*. doi: 10.1130/B36059.1.

Zhang ZM, Zhao, GC, Santosh M, Wang JL, Dong X and Shen K (2010) Late Cretaceous charnockite with adakitic affinities from the Gangdese batholith, southeastern Tibet: evidence for Neo-Tethyan mid-ocean ridge subduction?. *Gondwana Research* **17**, 615–31.

Zhao Z, Hu DG, Lu L and Wu ZH (2013) Discovery and metallogenic significance of the Late Cretacous adakites from Zetang, Tibet. *Journal of Geomechanics* **19**, 45–52 (in Chinese with English abstract).

Zheng YC, Hou ZQ, Gong YL, Wei L, Sun QZ, Zhang S, Fu Q, Huang KX, Li QY and Li W (2014) Petrogenesis of Cretaceous adakite-like intrusions of the Gangdese Plutonic Belt, southern Tibet: implications for mid-ocean ridge subduction and crustal growth. *Lithos* **190–191**, 240–63.

Zhong HT, Dai JG, Wang CS, Li YL and Wei YS (2016) Middle Jurassic-Early Cretaceous radiolarian assemblages of the western Yarlung-Zangbo Suture Zone: implications for the evolution of the Neo-Tethys. *Geoscience Frontiers* **8**, 989–97.

Zhou WD, Yang JS, Zhao JH, Ma CQ, Xiong FH, Xu XZ, Chen YH and Tian YZ (2015) Petrogenesis of peridotites from the Purang Ophiolite in western part of Yarlung-Zangbo Suture Zone, southern Tibet. *Acta Geologica Sinica (English Edition)* **89**, 125–6.

Zhu DC, Mo XX, Zhao ZD, Xu JF, Zhou CY, Sun CG, Wang LQ, Chen HH, Dong GC and Zhou S (2008) Zircon U-Pb geochronology of Zenong Group volcanic rocks in Coqen area of the Gangdese, Tibet and tectonic significance. *Acta Petrologica Sinica* **24**, 401–12 (in Chinese with English abstract).

Zhu DC, Pan GT, Mo XX, Wang LQ, Liao ZL, Zhao ZD, Dong GC and Yong C (2006) Late Jurassic-Early Cretaceous geodynamic setting in middle-northern Gangdese: new insights from volcanic rocks. *Acta Petrologica Sinica* **22**, 534–46 (in Chinese with English abstract).

Zhu DC, Zhao ZD, Niu YL, Mo XX, Chung SL, Hou ZQ, Wang LQ and Yuan WF (2011) The Lhasa terrane: record of a microcontinent and its histories of drift and growth. *Earth and Planetary Science Letters* **301**, 241–55.

Zhu DC, Zhao ZD, Pan GT, Lee HY, Kang ZQ, Liao ZL, Wang LQ, Li GM, Dong GC and Liu B (2009) Early Cretaceous subduction-related adakite-like rocks of the Gangdese Belt, southern Tibet: products of slab melting and subsequent melt–peridotite interaction? *Journal of Asian Earth Sciences* **34**, 298–309.